Modeling Key Pathways Proposed for the Formation and Evolution of “Cocktail”-Type Systems in Pd-Catalyzed Reactions Involving ArX Reagents

Polynskii, Mikhail; Ananikov, Valentine P.

DOI
10.1021/acscatal.9b00207

Publication date
2019

Document Version
Final published version

Published in
ACS Catalysis

ACS Catalysis

Research Article

Cite This: ACS Catal. 2019, 9, 3991−4005

pubs.acs.org/acscatalysis

Modeling Key Pathways Proposed for the Formation and Evolution of "Cocktail"-Type Systems in Pd-Catalyzed Reactions Involving ArX Reagents

Mikhail V. Polynski*[,†,‡,§] and Valentine P. Ananikov[‡,§,⊥]

[†]Department of Chemical Engineering, Delft University of Technology, Van der Maasweg 9, 2629 HZ Delft, The Netherlands

[‡]Faculty of Chemistry, Moscow State University, Leninskiye Gory, Moscow, 119991, Russia

[§]Zelinsky Institute of Organic Chemistry, Russian Academy of Sciences, Leninsky prospekt 47, Moscow, 119991, Russia

[⊥]Saint Petersburg State University, Universitetsky Prospect, 26, St. Petersburg 198504, Russia

Supporting Information

ABSTRACT: Reversible leaching of palladium nanoparticles occurs in a variety of catalytic reactions including cross-couplings, amination, the Heck reaction, etc. It is complemented by capturing of soluble palladium species on the surface of nanoparticles and de novo formation of nanoparticles from Pd precatalysts. We report here a detailed computational study of leaching/capture pathways and analysis of related stabilization energies. We demonstrate the validity of the "cocktail-of-species" model for the description of Pd catalysts in ArX oxidative-addition-dependent reactions. Three pools of Pd species were evaluated, including (1) the pool of catalytically active Pd nanoparticles with a high concentration of surface defects, (2) the pool of monomeric and oligomeric L[ArPdX]$_n$L species, and (3) the pool of irreversibly deactivated Pd. Stabilization by ArX oxidative addition, coordination of base species, and binding of X^- anions were found to be crucial for "cocktail"-type systems, and the corresponding reaction energies were estimated. An inherent process of ArX homocoupling, leading to the formation of Pd halides that require reactivation, was considered as well. The pool of irreversibly deactivated Pd comprises nanoparticles with (1 1 1) and (1 0 0) facets and Pd in the bulk form. The study is based on DFT modeling and specifies the role of Pd nanoparticles in (quasi-)homogeneous coupling reactions involving ArX reagents.

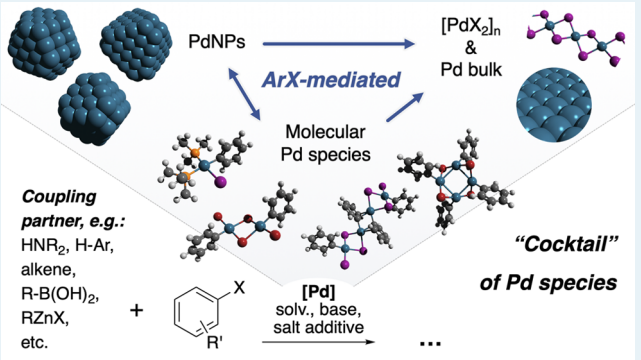

KEYWORDS: *Pd nanoparticles, cross-coupling catalysts, DFT modeling, catalyst evolution, oxidative addition, aryl halides, Pd leaching, Pd halides*

1. INTRODUCTION

The design of catalysts by computational modeling represents an influential trend in modern science.[1−4] It is a cutting-edge challenge which requires an in-depth understanding of the structure of active catalytic species, catalyst resting state(s), and catalyst deactivated forms, as well as factors that drive a catalytic process toward higher activity or deactivation (i.e., a model of catalytic system evolution is needed).[5,6] A comprehensive experimental description of such systems can be extremely difficult due to their dynamic nature.[5]

Computational chemistry provides unique tools for evaluation of the role of dynamic processes in catalysis. It inherently allows characterization of catalytic intermediates as short-lived species at ultralow concentrations that can hardly be detected with currently available experimental techniques. For this reason, computational modeling is very useful in the rational design of catalysts for a variety of synthetic processes.

Pd-catalyzed functionalization reactions are currently considered as one of the cornerstones of organic chemistry. Suzuki, Negishi, Kumada, and Sonogashira couplings as well as the Heck reaction, among many other synthetic transformations, allow efficient synthesis of many complex organic molecules.[7−18] Direct C−H-arylations seem even more promising in this regard, as they proceed without organometallic coupling partners (which may be expensive or toxic).[19−22] Cross-coupling strategies are highly efficient in molecular functionalization: e.g., the Buchwald−Hartwig amination and some other carbon−heteroatom bond formation reactions provide the well-established means for introduction of functional groups.[23−25] It is important to mention that transition-metal-catalyzed couplings have found

Received: January 16, 2019
Revised: March 19, 2019
Published: March 25, 2019

DOI: 10.1021/acscatal.9b00207
ACS Catal. 2019, 9, 3991−4005

their way to large-scale synthesis and are currently in demand in chemical industry.[26−29]

Historically, an initial approach was to introduce a Pd precatalyst in the form of a metal salt or metal complex into the reaction medium. Accordingly, the active sites proposed in the catalytic reaction mechanisms were monometallic.[30] After the activity of Pd clusters and nanoparticles had been discovered, the focus shifted to catalytic processes on the surface of metal particles.[22,31−36] It turned out, however, that both routes can be combined in complex catalytic systems, with a number of processes (leaching, redeposition, agglomeration, Ostwald ripening, etc.) promoting the formation of a "cocktail" of catalytic species and dynamic transformations of the system itself in the course of the reactions.[5,37−44]

When these modes of catalysis are considered in more detail, the following phenomena should be highlighted. The classic Pd precatalysts[45] in the form of Pd salts, as well as Pd complexes bearing seemingly tightly bound phosphine,[46] pincer,[47] or N-heterocyclic carbene ligands (NHC ligands),[48−52] release Pd species that participate in the formation of Pd nanoparticles (PdNPs) in the course of cross-coupling and functionalization reactions. This phenomenon is reflected in the concept of dynamic catalysis operated by the "cocktail" of catalytic species.[5] Currently, it is well established that PdNP precatalysts, initially seen as easily separable and highly active, are prone to the leaching of surface Pd into solution. The activity of these catalytic systems is attributed to the "leached Pd" in the solution phase. At the same time, PdNPs are considered as a reservoir of active species.[34,37,53−58] Palladium leaching is a reversible process, and its mechanistic counterpart is usually referred to as capture or redeposition.[5,59] All of these observations comprise the unified picture of Pd-catalyzed reactions with the central part of unclear chemical nature (Figure 1, left). Species, being intermediate to both Pd

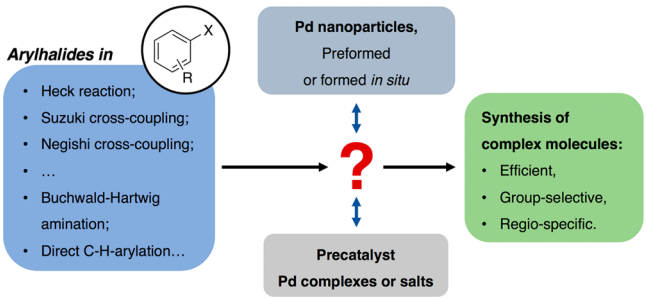

Figure 1. (left) Pd precatalysts (complexes and salts) and PdNPs undergo interconversions, leading to the dynamic mode of catalysis, in the course of transformations involving ArX reagents (blue double-sided arrows, see the text for discussion). (right) Key questions to be addressed.

nanoparticles and Pd complexes, are the "leached Pd". An understanding of their nature is essential for correct comprehension of Pd catalytic systems with the aforementioned dynamic properties.

Conventional approaches to the computational modeling of Pd-catalyzed cross-coupling and hydrogenation reactions have focused on Pd complexes as the primary catalytic species. These approaches are indispensable for our current understanding of catalytic phenomena (see refs 6, 30, and 60−64 for recent reviews). However, considerations of the leaching and capture/redeposition phenomena seem to be overlooked in theoretical studies. Studies by Heinz, Knecht, et al., performed with an empirical force-field method, should be mentioned as rather notable examples.[65−68] Moreover, the stabilization of the leached species (either by halide anions or due to the ligand or base coordination) was considered only for the case of an ionic liquid solvent.[69] A comprehensive evaluation of the whole variety of Pd species, as well as pathways to their stabilization, activation, and deactivation, is crucially important for the initiative of rational catalyst design.

In the present study, we use DFT computations to investigate the energetics of a "cocktail"-type system formation. We model a variety of Pd species that coexist in the system, with a particular focus on the identification of stabilizing factors. In addition, we describe some inherent deactivation pathways that are peculiar to the studied system (Figure 1, right). The reported computational research provides a comprehensive model of Pd catalytic systems in reactions that involve leaching and aryl halide (ArX) oxidative addition (OA). It substantially improves our understanding of the influence of these processes on the evolution of the systems in the course of cross-coupling and functionalization reactions.

2. COMPUTATIONAL DETAILS

Binding of ligands or aryl halide (ArX) oxidative addition to the Pd nanoparticle surface ($\Delta E'_{bind}$) are known to initiate leaching ($\Delta E'_{det}$, Figure 2).[31,47,58,65,67,70,71] In this work, we modeled the entire process of leaching (ΔE_{leach}) as the following set of steps. The first one was detachment of molecular Pd species (ΔE_{det}), then binding of ligands (ΔE_{bind}) and (or) oxidative addition (ΔE_{OA}) of ArX to the species, and subsequent oligomerization of the species (ΔE_{oligo}):

$$\Delta E_{leach} = \Delta E_{det} + \Delta E_{bind} + \Delta E_{OA} + \Delta E_{oligo} = \Delta E_{det} + \Delta E_{stab} \quad (1)$$

$$\Delta E_{stab} = \Delta E_{bind} + \Delta E_{OA} + \Delta E_{oligo}$$

Considering the chosen model system in more detail, we calculated detachment energies (E_{det}, endothermic) of Pd atoms and clusters (Pd_2 and Pd_4) from Pd_n nanoparticles (n = 79, 116, 140). The exothermic effect of the stabilizing processes (ΔE_{stab}) in the *N*,*N*-dimethylformamide solvent (DMF) was estimated via a consideration of binding energies of representative ligands (NMe_3, PMe_3, Br^-, and I^-; E_{bind}, exothermic) and energies of PhBr and PhI oxidative addition (E_{OA}, exothermic) to the detached species and the oligomerization energy (E_{oligo}, exothermic) of the leached species. By considering this simple set of elementary reactions, we model leaching in a continuous regime (see section 7 of the Supporting Information for details).

The endothermic part was estimated via non-spin-polarized DFT computations (PBE functional)[72] performed using the VASP 5.3.3 program.[73] A plane-wave basis set with a cutoff energy of 415 eV and the projector augmented wave method (PAW) were used.[74] Brillouin zone sampling was restricted to the γ point in all cases except for the case of the Pd bulk modeling. In the latter case, Pd supercells containing 27 and 26 atoms were constructed from the face-centered cubic unit cell, and the Monkhorst−Pack sampling[75] of the Brillouin zone with a 9 × 9 × 9 mesh was chosen. Fermi−Dirac[76] smearing with a broadening width of 0.1 eV was applied to improve the convergence.

DOI: 10.1021/acscatal.9b00207
ACS Catal. 2019, 9, 3991−4005

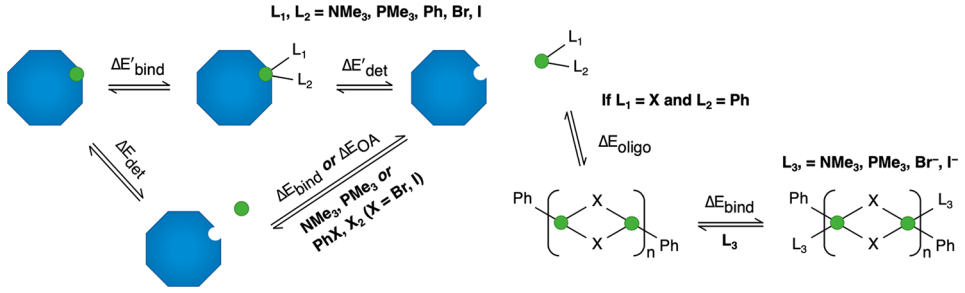

Figure 2. Possible leaching, capture, and oligomerization processes in Pd catalytic systems. Pd nanoparticles are shown in blue and detached Pd atoms or clusters in green.

To estimate the exothermic contributions, the ORCA 3.0.3 program was used to perform restricted Kohn–Sham DFT calculations with the PBE functional.[77] We used the broken-symmetry DFT approach to obtain consistent results in modeling of singlet Pd_n (n = 1–4) species (see the Supporting Information for details). The def2-TZVPD basis set including diffuse exponents and the resolution-of-identity (RI) approximation were used.[78−84] To model the core electron shells in Pd and I atoms, the Stuttgart–Dresden "def2-SD" effective core potentials were selected.[85,86] Bulk solvent effects were modeled by using the COSMO implicit solvent model (with standard parameters for the DMF solvent).[87]

The complete computational setup, including the details of the transition state search procedure, is presented in the Supporting Information. Only singlet states were considered (see discussion in section 9 of the Supporting Information). We abstained from using empirical dispersion corrections in this particular case (see the rationale in sections 9.1 and 9.2 of the Supporting Information). DFT-PBE computations with a plane-wave basis set and the PAW method offered exceptional accuracy in calculations of Pd metal properties.[88] Plane-wave DFT computations are computationally cheaper yet generally more accurate in the modeling of transition-metal nanoparticles in comparison with the Gaussian basis set counterparts.[89] On the other hand, calculations at the PBE/aug-cc-pVDZ(-PP) level of theory represented well the ligand binding energies in *cis*- and *trans*-$[L\text{-}Pd(PH_3)_2Cl]^+$ complexes computed at the CCSD(T)/aug-cc-pVTZ(-PP) level of theory.[90] It was also shown that PBE/triple-ζ//BP86/triple-ζ could be an optimal choice for computation of ligand substitution energies in solution.[91] DFT computations with Gaussian basis sets allow modeling (quasi-)periodic systems with large vacuum layers to be avoided as well as allow straightforward modeling of charged systems. Therefore, we combined plane wave and Gaussian basis set computations in this work. Since different wave function approximations were used for the estimations of the endothermic (E_{det}) and exothermic (E_{bind}, E_{OA}, and E_{oligo}) terms, an additional test was performed to ensure consistent results (see section 9.3 of the Supporting Information).

A note should be given regarding free energy computations. Although being expensive in terms of CPU time, molecular dynamics (QM/MM or fully ab initio) is an informative and efficient approach for this task, as was shown in theoretical studies of homogeneous Pd catalysts.[69,92−98] This computational approach in our case would require constructing hundreds of explicit solvent model systems and performing corresponding costly MD runs. Conventional quantum chemical calculations of free energies with implicit solvent models can be accurate within several kcal/mol, in comparison to AIMD. However, free energy calculations with conventional implicit solvent models can give misleading predictions due to incorrect estimation of solution-phase entropy terms.[99] Moreover, it is unclear how to consistently and accurately compute the free energy of leaching and capture using an implicit solvent model and conventional statistical thermodynamics approach (as long as solid–liquid interface thermodynamics is involved). Major corrections to the computed energies that we present below result from the gain in translational entropy (to the E_{det} term) and the loss in translational entropy (to the E_{bind}, E_{OA}, and E_{oligo} terms). Notably, the loss/gain corrections in our case have opposite signs, while the predicted speciation of the "leached Pd" in solution is in accordance with experimental observations (see section 3.1). As the first step in the formulation of the theory of "cocktail"-type catalytic systems, we avoided considering free energies and barriers of detachment of molecular Pd species from the PdNP surface, focusing the discussion on the energetics of leaching.

3. RESULTS AND DISCUSSION

3.1. Detachment from Pd Nanoparticles. Detachment energies (E_{det}) of molecular Pd species Pd_n (n = 1, 2, 4) from Pd_m nanoparticles (m = 79, 116, 140) were modeled according to eq 2, where Pd_{m-n} is a palladium nanoparticle after the detachment of a Pd_n cluster or atom. N_{broken} is the number of Pd–Pd bonds broken in the process.

$$E_{det}:\ Pd_m \rightarrow Pd_{m-n} + Pd_n \qquad (2)$$

The detachment of the nonequivalent atoms from the cuboctahedral Pd_{79} and Pd_{140} nanoparticles (cut from the Pd bulk by (1 1 1) and (1 0 0) planes) and the octahedral Pd_{116} nanoparticle (cut from the bulk by the (1 1 1) plane) was considered (see Figure 3). E_{det} increases with an increase in N_{broken} (Table 1). Vertex atoms have the lowest coordination number (N_{broken} = 6) in comparison with edge atoms (N_{broken} =

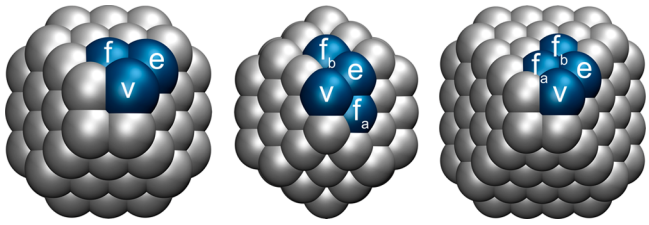

Figure 3. Considered Pd_{79}, Pd_{116}, and Pd_{140} nanoparticles. Nonequivalent vertex, edge, and facet atoms are shown in blue and denoted as v, e, and f_a and f_b, respectively.

DOI: 10.1021/acscatal.9b00207
ACS Catal. 2019, 9, 3991−4005

Table 1. Computed Detachment Energies (E_{det}, kcal/mol) of Pd Atoms from Pd_{79}, Pd_{116}, and Pd_{140} Nanoparticles

Pd_{79}			Pd_{116}			Pd_{140}		
Pd atom position	E_{det}	N_{broken}	Pd atom position	E_{det}	N_{broken}	Pd atom position	E_{det}	N_{broken}
v	82.9	6	v	84.6	6	v	83.5	6
e	91.1	7	e	92.3	7	e	93.8	7
f	102.4	9	f_a	102.8	9	f_a	101.7	9
			f_b	98.4	8	f_b	104.8	9
Pd bulk	115.1	12						

7) and facet atoms (N_{broken} = 9). Isolation of a Pd atom from the bulk leads to a cleavage of 12 Pd−Pd bonds and is endothermic by 115.1 kcal/mol.

The same relationship between E_{det} and N_{broken} is observed for the detachment of Pd_2 and Pd_4 species. At least 135.0 kcal/mol is required to detach Pd_2 (two adjacent vertex Pd atoms) from a (1 0 0) facet of the Pd_{79} nanoparticle by breaking 10 Pd−Pd bonds. The least endothermic (155.2 kcal/mol) detachment of Pd_4 (the quartet forming a (1 0 0) facet) from the Pd_{79} nanoparticle is associated with the cleavage of 14 Pd−Pd bonds (see the Supporting Information for E_{det} values and corresponding structures).

The relationship between E_{det} and N_{broken} for the case of atom-by-atom detachment may be approximated with the following function (see the Supporting Information for details of the approximation):

$$E_{det} = 44.68n + 6.62N_{broken} \quad (3)$$

where n is the number of detached Pd atoms. Note that if no atoms are detached, n = 0 and N_{broken} = 0; hence, E_{det} = 0.

Equation 3 allows us to calculate E_{det} with a root-mean-square deviation (RMSD) of 1.8 kcal/mol and mean absolute deviation (MAD) of 1.5 kcal/mol (in comparison to the aforementioned plane-wave DFT computations). We assume that the endothermic effect of detachment (E_{det}) must be fully compensated by the total exothermic effect of ligand binding, oxidative addition, and oligomerization of soluble molecular Pd species (E_{bind} + E_{OA} + E_{oligo}, Figure 2):

$$E_{det} + E_{bind} + E_{OA} + E_{oligo} \leq 0 \quad (4)$$

On the basis of this rule, we can define the *maximal number of Pd−Pd bonds cleaved upon leaching* (N_{max}) as a minimal integer that gives minimal E_{det} in eq 4 for a given number of detached atoms n and the E_{bind} + E_{OA} + E_{oligo} sum. We used eqs 3 and 4 to calculate N_{max} and N_{max}/n for every considered molecule below (see the Supporting Information for further details). We also propose N_{max}/n as a metric of stability of leached species in terms of their resistance to being recaptured at the Pd nanoparticle surface.

The minimal value of N_{max} was chosen to be 3 per detached atom (matching n in the case of Pd adatoms on the (1 1 1) Pd surface). The maximal value of 12 bonds per detached atom corresponds to the hypothetical case of Pd atom isolation from the bulk. Since every Pd atom of the (1 0 0) surface has 8 closest neighbors (N_{broken}, see Table 1) and every atom of a (1 1 1) facet has 9 neighbors:

$$N_{max}/n \geq 9$$

This indicates that leached molecular species are highly resistant to recapture; i.e., the species most improbably redeposit at the surface of Pd nanoparticles considering that the (1 0 0) and (1 1 1) faceted surfaces are the most stable.[100]

As we have already mentioned, the observed catalytic activity of Pd in reactions involving ArX reagents is generally attributed to leached Pd species in solution.[34,37,53−56] Pd nanoparticles with (7 3 0) and (2 2 1) high-index facets have been reported as highly active in cross-coupling and Heck reactions. They provide at least a 2-fold increase in activity (measured in turnover numbers) in comparison with nanoparticles that have (1 1 1) and (1 0 0) facets only.[35,37,55] The boosted activity is attributed to facile leaching of Pd atoms from (7 3 0) and (2 2 1) high-index facets, as they are composed of low-coordinated Pd atoms (N_{broken} = 4, 5, respectively).[37,55] Although Pd nanoparticles with (1 1 1) and (1 0 0) low-index facets (N_{broken} = 9, 8, respectively) can also act as catalysts, their activity may be due to leaching of edge and vertex Pd atoms, as well as Pd adatoms and the atoms located at surface defects.

Anionic mono- and dipalladium species reportedly form catalytic intermediates in cross-coupling and functionalization reactions[54,101−109] (see structures (174), (175), (185), (187), (189), and (191) in the Supporting Information). Thus, in active catalytic systems, the presence of anionic species in solution is expectable. The species (174), (175), (185), (187), (189), and (191) have N_{max}/n values of 4.5−6.0, which is close to N_{broken} = 4−5, as in the case of (7 3 0) and (2 2 1) facets that are prone to facile leaching according to experimental findings. Therefore, N_{max}/n values within the range of

$$4.5 \leq N_{max}/n < 8$$

should indicate the presence of a particular molecule in solution under operating catalytic conditions. In fact, a "cocktail" of various species may have an N_{max}/n value lying in this interval (see below); these species are hereafter referred to as "leached Pd".

According to the proposed model, an equilibrium value of the leaching−capture Gibbs free energy (ΔG_{leach}) under the given conditions (reactants, solvent, temperature, etc.) does not necessarily correspond to an exergonic mode. Typically, 0.5−300 ppm amounts of leached palladium (ω_{Pd}) are present in the reaction medium.[34,55,56,110−114] Chemical equilibrium at conditions that involve ΔG_{leach} is described as

$$\Delta G_{det}: \ NP \rightleftharpoons NP^* + Pd_n$$

$$K_{eq} = \frac{[NP^*][Pd_{mol}]}{[NP]}$$

[NP] and [NP*] are the activities of a pristine nanoparticle and a nanoparticle after detachment of a small Pd_n cluster, respectively, and [Pd_n] denotes the activity of the detached cluster. We assume that [NP] ≈ [NP*], as long as the nanoparticle has a similar structure before and after the detachment (in the case of a single leaching event; i.e. the particle neither dissolves nor significantly degrades but

DOI: 10.1021/acscatal.9b00207
ACS Catal. 2019, 9, 3991−4005

Table 2. Computed Binding Energies of NMe_3 and PMe_3 to Pd_n species (n = 1, 2, 4) in kcal/mol[a]

	E_{bind}(DMF)			E_{bind}(DMF)			E_{bind}(DMF)	
k	Pd_1 + $k$$NMe_3$	Pd_1 + $k$$PMe_3$	k	Pd_2 + $k$$NMe_3$	Pd_2 + $k$$PMe_3$	k	Pd_4 + $k$$NMe_3$	Pd_4 + $k$$PMe_3$
1	−24.4 (0)	−55.9 (0)	1	−28.8 (0)	−67.9 (0)	1	−19.4 (0)	−38.1 (0)
2	−53.3 (0)	−93.8 (7)	2	−58.0 (0) to −56.2 (0)	−108.9 (3) to −107.9 (3)	2	−33.1 (0) to −28.8 (0)	−74.2 (0) to −71.8 (0)
3	no binding	−103.0 (8)	3	−77.8 (0)	−144.2 (6)	3	−55.4 (0) to −41.2 (0)	−126.9 (3.75) to −121.3 (3.5)
4		−110.9 (9)	4	Pd−Pd bond cleavage	−161.0 (7) to −157.2 (7)	4	−68.8 (0) to −44.8 (0)	−165.6 (5.25)
			5		−165.6 (7.5)	5	No binding	−182.1 (5.75) to −179.6 (5.75)
			6		Pd−Pd bond cleavage	6		−193.9 (6.25)
						7		−198.2 (6.5)
						8		−198.9 (6.5)

[a] N_{max}/n metric values are given in parentheses; k is the number of ligands bound to a Pd cluster or atom in a given transformation.

preserves its morphology). If we apply the ideal solution approximation, then $[Pd_n]$ is equal to the concentration of soluble palladium species c_{Pd} and

$$\Delta G_{leach} = -RT \ln(c_{Pd})$$

Concentration of soluble palladium species may be estimated via

$$\omega_{Pd} = \frac{m_{Pd}}{m_{react}} = \frac{n_{Pd}M_{Pd}}{\rho_{react}V_{react}} = c_{Pd}\frac{M_{Pd}}{\rho_{react}}$$

where m_{Pd} and m_{react} are masses of soluble palladium species and reaction medium, respectively, n_{Pd} is the amount of soluble Pd, V_{react} is the reaction medium volume, M_{Pd} is the molar mass of soluble palladium species, and ρ_{react} is reaction medium density. Therefore

$$\Delta G_{leach} = -RT \ln\left(\omega_{Pd}\frac{\rho_{react}}{M_{Pd}}\right) \quad (5)$$

Since the ρ_{react}/M_{Pd} term is logarithmic, the effect of solvent density and molar mass of leached species on ΔG_{leach} is minor (within about 1 kcal/mol in exemplary cases discussed in section 2 of the Supporting Information). However, an increase in ΔG_{leach} by about 7 kcal/mol makes a qualitative difference. It may reduce leaching (ω_{Pd}) ~10^5 times, as breaking of an additional Pd−Pd bond upon detachment requires about 6.6 kcal/mol according to eq 3.

Hence, the leaching−capture equilibrium is extremely sensitive to N_{broken} in the model case of an ideally regular Pd nanoparticle surface. Palladium adatoms are the most prone to leaching, followed by edge and vertex atoms and the atoms of high-index facets. This sensitivity to N_{broken} should be accounted for in nanocatalyst design, as the available NP synthesis techniques allow synthesis of nanoparticles with predefined Miller index facets.[35,71,115] After all Pd atoms from such high-index facets have leached, the remaining regular (1 1 1) and (1 0 0) facets are overstable and give no significant contribution to the pool of highly active soluble Pd species.

3.2. Ligand Binding and Oxidative Addition to Molecular Pd Species. We started our consideration of the exothermic reactions depicted in Figure 2 by computing binding energies (E_{bind}) for binding of NMe_3 and PMe_3 to Pd_n (n = 1, 2, 4) in DMF (see the Supporting Information for E_{bind} values under vacuum). PMe_3 is often selected as a model ligand in computational studies of catalytic cross-coupling reactions.[62,63,116−123] Notably, the ligand binding energies in $[Pd(PMe_3)]$ and $[Pd(PPh_3)]$ species computed at the ZORA-BLYP-D3/TZ2P level of theory differ by only 0.7 kcal/mol, while the largest difference is observed in the $[P(PMe_3)]$ vs $[P(PCy_3)]$ case (−49.0 vs −53.5 kcal/mol, respectively).[124] Therefore, the PMe_3 ligand can be considered as a representative model of a phosphine ligand imposing moderate steric hindrance. NMe_3 is a model of a typical nitrogen base that is commonly used under experimental catalytic conditions.

To model the binding, PMe_3 and NMe_3 molecules were placed near to Pd_n (n = 2, 4) until the geometry optimization procedure resulted in no valent Pd−N binding or in Pd−Pd bond cleavage: i.e., until the structure of the Pd_n (n = 2, 4) clusters remained qualitatively unchanged. The obtained binding energies are given in Table 2. Trimethylamine (NMe_3) has shown a relatively low binding affinity, and up to two NMe_3 molecules can bind to one Pd atom. Binding of the fourth NMe_3 molecule to Pd_2 leads to Pd−Pd bond cleavage, while in the case of Pd_4 only one NMe_3 per Pd atom can be bound in the maximally saturated state. Expectedly, PMe_3 has a higher binding affinity to Pd_n (n = 1, 2, 4) and may bind in the μ_2 and μ_3 bridging configurations. For comparison, NMe_3 was bound to Pd_2 and Pd_4 in only a μ_1 configuration (Figure 4, see the Supporting Information for all considered $[Pd_nL_m]$ structures, L = NMe_3, PMe_3).

We have estimated the stabilizing effect (N_{max}/n) of NMe_3 and PMe_3 ligands on Pd_n (n = 1, 2, 4) (see Table 2). Due to the relatively low binding affinity, NMe_3 cannot stabilize Pd_n (n = 1, 2, 4) to prevent its recapture at the surface (all N_{max}/n values are zero). Trimethylphosphine, on the other hand, stabilizes Pd_n (n = 1, 2, 4) much better, as the expected catalytic species $[Pd(PMe_3)_2]$ (Figure 4) are resistant to recapture at the edges. Four PMe_3 ligands stabilize Pd so effectively that the formation of the Pd (1 1 1) surface becomes thermodynamically unfavorable (Table 2). Pd_4 clusters can bind up to eight PMe_3 ligands; the resulting $[Pd_4(PMe_3)_8]$ clusters are relatively stable (N_{max}/n = 6.5). The estimation of kinetic stability is beyond the scope of this study. Nevertheless, given that species containing Pd_{3-4} cluster cores are reportedly active,[56,125] moderate resistance of the phosphine-stabilized Pd_4 clusters to recapture at the PdNP surface indicates the possibility of their persistence under catalytic conditions.

Aryl halides are seen as the key agents that drive Pd leaching into solution.[31,53,66,67,70,126] To assess their stabilizing effect, oxidative addition of PhBr and PhI to Pd_n (n = 1, 2, 4) in DMF or under vacuum was modeled (see Table 3 for the OA in DMF and the Supporting Information for the OA under vacuum). The calculations have shown that affinities (E_{OA}) of PhBr and PhI to Pd atoms are similar to the affinity of PMe_3 and higher than the affinity of NMe_3. It is worth noting that only oxidative addition of two PhI molecules to a Pd atom

DOI: 10.1021/acscatal.9b00207
ACS Catal. 2019, 9, 3991−4005

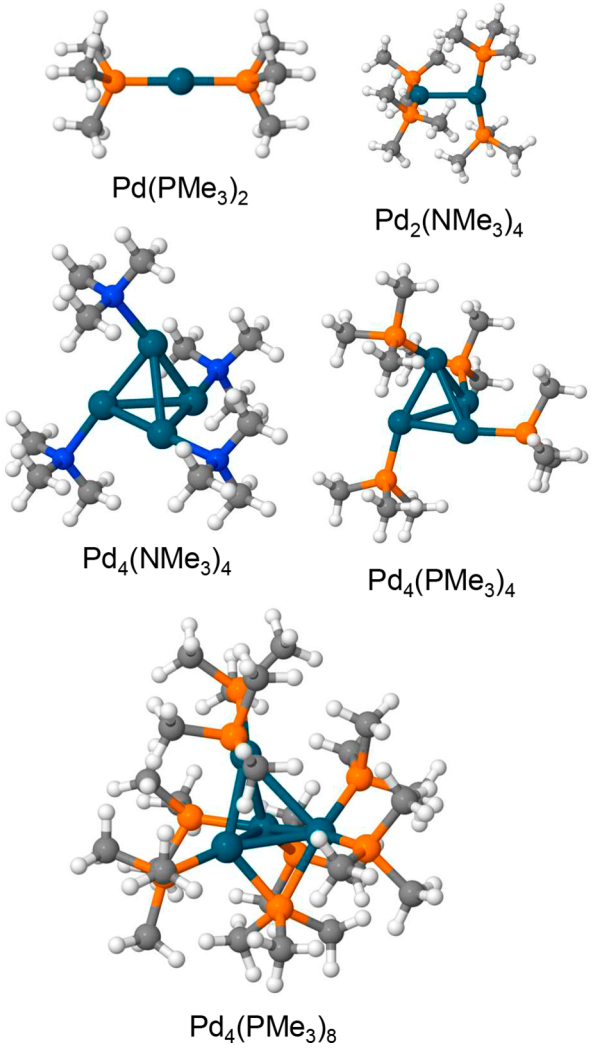

Figure 4. Representative optimized structures of $[Pd_nL_m]$ (L = NMe_3, PMe_3) species. Pd is shown in cerulean, H in white, C in gray, N in blue, and P in orange.

results in any significant stabilizing effect (N_{max}/n = 3). Therefore, aryl halides alone cannot effectively stabilize molecular Pd in solution, although they play a central role in the considered stabilization processes (see the next section).

Calculated energies of Br_2 and I_2 oxidative additions are given in Table 3. Considering rationalization for modeling of this step, it is proposed that I_2 forms under reaction conditions and takes part in $[Pd_2I_6]^{2-}$ formation.[70,101] An alternative pathway of PdX_2 formation, i.e. formation of PdI_2 via a reductive elimination of Ph−Ph from $[Ph_2PdX_2L_{0-2}]$ species, is also possible. The latter pathway appears to be both thermodynamically favorable and kinetically feasible according to our modeling results (Figure 5).

PhPdX species **1** can undergo three different pathways in the model system (the pathways are marked with green, blue, and red in Figure 5; see section 8 of the Supporting Information for a detailed scheme and the energetics). Excess of aryl halide reagent, relative to ArPdX, L, and X^- species (red sector in Figure 5), may lead to formation of unstable Pd(IV) complexes (**2**, **6**, **7**, **9**). The complexes **2**, **6**, **7**, and **9** are products of two consecutive PhX oxidative additions to Pd. The second OA step proceeds with the barriers in the range from 7 to 18 kcal/mol depending on the ligands bound to the transition metal centers (see section 8 in the Supporting Information). The Pd(IV) complexes can readily undergo reductive elimination of biphenyl (**2** → **13**, **7** → **12**, **6** → **10**, and **9** → **11**) with the barriers in the range from 4 to 18 kcal/mol. Since a second coupling partner is added to a catalytic system under experimental conditions (for example, arylboronic acid in Suzuki coupling etc.), the pathway to the Pd(IV) species formation and the concomitant aryl halide homocoupling is normally avoided.

A path to avoid the homocoupling process is binding of an X^- anion or a ligand with subsequent formation of $L[PhPdI]_nL$ oligomers (blue sector in Figure 5, see section 3.3 for a discussion of $L[PhPdI]_nL$ oligomer formation). Another possible path is binding of PMe_3 or NMe_3 species that leads to formation of L[PhPdX]L complexes and, subsequently, can initiate the classic Pd(0)/Pd(II) catalytic cycle (green sector in Figure 5). In real catalytic systems, homocoupling rate vs cross-coupling rate is determined by aryl halide reactivity, coupling partner reactivity, stabilizers (here, L and X^- species), and reaction conditions. Nevertheless, too large an excess of ArX reagent should not be used, as it may stimulate formation of Pd(II) halide species **10**−**12** (well-known catalyst precursors that require reactivation) and homocoupling products.

Leaching is facile as an atom-by-atom process, according to the computations presented above. Covalent Pd−Pd bonds are weak in comparison with the metallic bonds. The endergonic effect of the metallic Pd−Pd bond breaking can be balanced by the stabilizing effect of the covalent Pd−heteroatom and Pd−Pd bond formation in leached molecular species (see eq 1). The cohesive energy of Pd_4 is −38.0 kcal/mol per atom, while the cohesive energies of the considered Pd_{79} and Pd_{140} nanoparticles are −69.1 and −72.2 kcal/mol per atom, respectively (DFT-PBE, plane-wave basis set, and PAW

Table 3. Computed Energies of PhBr, PhI, PhPh, Br_2, and I_2 Oxidative Addition to Pd_n Species (n = 1, 2, 4) in kcal/mol[a]

reaction	E_{OA}(DMF)	reaction	E_{OA}(DMF)	reaction	E_{OA}(DMF)
Pd_1 + Br_2	−65.1, −68.7[b] (3)	Pd_2 + Br_2	−99.8 (0)	Pd_4 + Br_2	−79.4 (0) to −64.9 (0)
Pd_1 + I_2	−60.5, −81.3[b] (0)	Pd_2 + I_2	−98.4 (0)	Pd_4 + I_2	−75.9 (0) to −73.7 (0)
Pd_1 + PhBr	−49.4 (0)	Pd_2 + PhBr	−79.2 (0)	Pd_4 + PhBr	−47.0 (0)
Pd_1 + 2PhBr	−63.3, −13.9[c] (0)			Pd_4 + 2PhBr	−114.2 (3.25) to −75.8 (0)
Pd_1 + PhI	−54.4 (0)	Pd_2 + PhI	−87.8 (0)	Pd_4 + PhI	−58.9 (0)
Pd_1 + 2PhI	−68.6, −14.2[c] (3)			Pd_4 + 2PhI	−127.5 (3.75) to −93.9 (0)
Pd_1 + PhPh	−15.0 (0)	Pd_2 + PhPh	−45.6 (0)	Pd_4 + PhPh	−27.2 (0) to −20.3 (0)

[a] N_{max}/n metric values are given in parentheses. [b] Comma-separated energies of one-step X_2 oxidative addition and PdX_2 formation from $[Ph_2PdX_3]^-$ through the Ph−Ph reductive elimination pathway (see text). [c] Comma-separated total energy of the oxidative addition of two PhX molecules and energy of the second PhX molecule addition.

DOI: 10.1021/acscatal.9b00207
ACS Catal. 2019, 9, 3991−4005

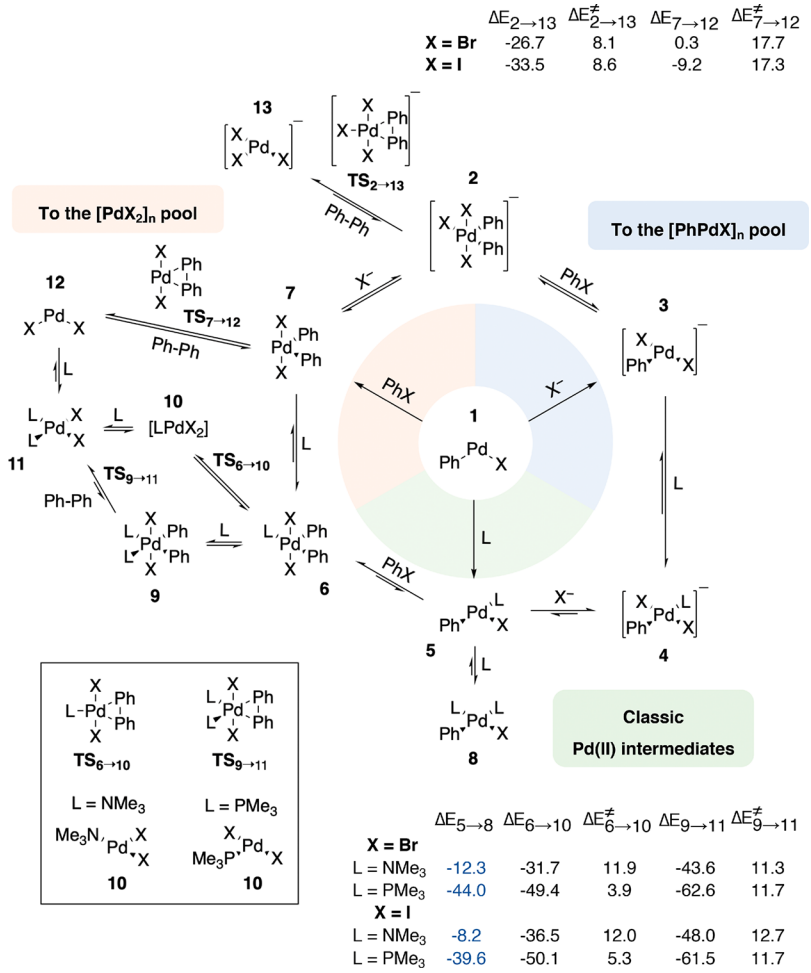

	$\Delta E_{2\rightarrow13}$	$\Delta E^{\neq}_{2\rightarrow13}$	$\Delta E_{7\rightarrow12}$	$\Delta E^{\neq}_{7\rightarrow12}$
X = Br	-26.7	8.1	0.3	17.7
X = I	-33.5	8.6	-9.2	17.3

	$\Delta E_{5\rightarrow8}$	$\Delta E_{6\rightarrow10}$	$\Delta E^{\neq}_{6\rightarrow10}$	$\Delta E_{9\rightarrow11}$	$\Delta E^{\neq}_{9\rightarrow11}$
X = Br					
L = NMe_3	-12.3	-31.7	11.9	-43.6	11.3
L = PMe_3	-44.0	-49.4	3.9	-62.6	11.7
X = I					
L = NMe_3	-8.2	-36.5	12.0	-48.0	12.7
L = PMe_3	-39.6	-50.1	5.3	-61.5	11.7

Figure 5. Excess of $[PhPdXL_{0-1}]$, PhX, NMe_3, PMe_3, or X^- directs a Pd catalytic system to follow three distinct pathways. See section 9.2 of the Supporting Information for details of the transition state searching procedure. See a discussion of the $[PhPdX]_n$ and $[PdX_2]_n$ pool formation in the text.

method; see the Supporting Information for a detailed description of the computational parameters). Pd atoms in molecular subnanometer Pd clusters are bound with relatively weak Pd−Pd bonds of covalent nature. A thermodynamically favorable way involves the atom-by-atom detachment with subsequent exothermic formation of up to four strong covalent bonds with various ligands and/or oxidative addition of ArX, as well as possible oligomerization of the products of the detachment. The last three processes can compensate for the endothermicity of the detachment, as we demonstrate in the next section.

3.3. Oligomerization of Leached Species and Binding of Additional Ligands. Arylpalladium halide species [ArPdX] may undergo two possible processes leading to their stabilization in solution. The first one is oligomerization; [ArPdX] may bind to another valence-unsaturated [ArPdX] molecule or to $[ArPdX_2]^-$. Dimeric and monomeric $[ArPdX]_n$ and $[ArPdX_2]^-$ species were observed in cross-coupling, Heck, and amination reactions.[54,102−109,127,128] $[PhPdX]_2$ dimers have three isomers, since phenyl rings may bind to transition-metal atoms in σ as well as in π binding mode (see Figure 6). μ_2 binding of aryl groups in M(II)−M(II) species was observed in Ni-catalyzed Kumada-type coupling.[129] Dipalladium species with bridging aryl ligands are

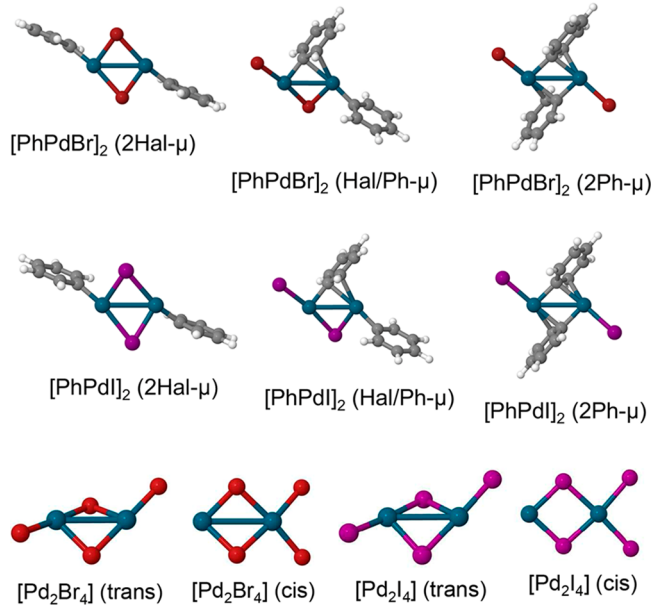

Figure 6. Optimized structures of $[PhPdX]_2$ and $[Pd_2X_4]$ (X = Br, I) isomers. See Table 4 for the corresponding dimerization energies. Pd is shown in cerulean, H in white, C in gray, Br in red, and I in violet.

DOI: 10.1021/acscatal.9b00207
ACS Catal. 2019, 9, 3991−4005

rarely observed; a few reports on these species belong to the field of Pd(I) chemistry.[130,131]

We modeled the formation of $[PhPdX]_{2-5}$ (X = Br, I) oligomers in DMF and under vacuum (see the Supporting Information for all obtained oligomer structures and corresponding E_{oligo} values); computed dimerization energies of $[PhPdX]_2$ (X = Br, I) are given in Table 4. Unexpectedly, a

Table 4. Computed Dimerization Energies (E_{oligo}, kcal/mol) and Corresponding N_{max}/n values of $[PhPdX]_2$ and $[Pd_2X_4]$ (X = Br, I) Isomers[a]

dimer	E_{oligo}(DMF)	N_{max}/n
$[PhPdBr]_2$ (2X-μ)	−23.4	0
$[PhPdBr]_2$ (X/Ph-μ)	−30.2	0
$[PhPdBr]_2$ (2Ph-μ)	−39.9	3.5
$[PhPdI]_2$ (2X-μ)	−26.3	3
$[PhPdI]_2$ (X/Ph-μ)	−31.0	3.5
$[PhPdI]_2$ (2Ph-μ)	−34.9	4
$[Pd_2Br_4]$ (trans)	−39.9	6.5
$[Pd_2Br_4]$ (cis)	−30.9	5.5
$[Pd_2I_4]$ (trans)	−40.5	8.5
$[Pd_2I_4]$ (cis)	−33.4	8

[a]See Figure 6 for the structures; N_{max}/n = 0 shows entries below the threshold (3 per detached atom).

bridging Ph group allows for stronger binding in comparison with I and Br groups; least-squares-fit binding energies are −11.5 and −19.7 kcal/mol per Br and Ph bridge groups in $[PhPdBr]_2$, respectively. In $[PhPdI]_2$, the binding energies were −13.2 and −17.5 kcal/mol for I and Ph bridging ligands, respectively. Evidently, the binding strength of bridging ligands in $[PhPdX]_n$ oligomers significantly depends on the chemical environment of the Pd atoms; for instance, the binding strengths of Ph groups differ by 2.2 kcal/mol in $[PhPdBr]_2$ and $[PhPdI]_2$. The formation of oligomeric halide $[Pd_nX_{2n}]$ (X = Br, I) species was modeled as well (see Table 4 for the case of $[Pd_2X_4]$ and the Supporting Information for all computed values). These species can oligomerize in two different configurations that we denote as cis and trans (Figure 6).

While the oligomerization itself makes molecular $[PhPdX]_2$ species more stable in solution (Table 4, rows 3−6, N_{max} = 3−4), stronger stabilization is provided by binding of X^- anions that may be formed in the course of the reaction, e.g. the Heck reaction, or introduced into the system with salt additives. Another way of stabilization is binding of NR_3 species (that are often added as a base; here modeled with NMe_3) or phosphine ligands PR_3 (here modeled with PMe_3). The corresponding binding energies of X^- to $[PhPdX]_{1-4}$ (X = Br, I; in DMF) and of L (L = NMe_3, PMe_3) to $[PhPdX]_{1-3}$ (in DMF and in vacuo) were computed. The binding energies for mono-Pd [PhPdX] species are discussed in the text; the trends are preserved in the case of $[PhPdX]_{2-4}$ species (see the Supporting Information for all computed E_{bind} values in DMF and in vacuo). As in the case of oligomerization, E_{bind} values strongly depend on the chemical environment of the Pd atom which undergoes the ligand binding process (see Table 5). Generally, X^- (X = Br, I) has as a strong binding affinity to $[PhPdX]_n$ as NMe_3. We selected N_{max} = 4.5 as the lower margin of stability (to fast capture back to the Pd surface, section 3.1). The binding of X^- and NMe_3 alone is exothermic enough to make monomeric L[PhPdX]L species stable in solution (N_{max} = 5). Binding of trimethylphosphine PMe_3

Table 5. Computed Binding Energies (E_{bind}) of X^- (X = Br, I) and L (L = NMe_3, PMe_3) to [PhPdBr] and [PhPdI] in kcal/mol

ligand binding reaction	E_{bind}(DMF)	N_{max}
$[PhPdBr] + Br^- = [PhPdBr_2]^-$	−29.2	5
$[PhPdI] + I^- = [PhPdI_2]^-$	−28.2	5
$[PhPdBr] + NMe_3 = [PhPdBr]NMe_3$	−20.7	3
$[PhPdBr]NMe_3 + NMe_3 = NMe_3[PhPdBr]NMe_3$	−12.5	5
$[PhPdBr] + PMe_3 = [PhPdBr]PMe_3$	−29.8	5
$[PhPdBr]PMe_3 + PMe_3 = PMe_3[PhPdBr]PMe_3$	−44.0	11
$[PhPdI] + NMe_3 = [PhPdI]NMe_3$	−20.9	4
$[PhPdI]NMe_3 + NMe_3 = NMe_3[PhPdI]NMe_3$	−8.6	5
$[PhPdI] + PMe_3 = [PhPdI]PMe_3$	−30.6	6
$[PhPdI]PMe_3 + PMe_3 = PMe_3[PhPdI]PMe_3$	−39.4	12
$PdBr_2 + Br^- = [PdBr_3]^-$	−34.8	8
$PdI_2 + I^- = [PdI_3]^-$	−31.4	10

ligands to [PhPdI] species leads to exceptionally strong stabilization in the form of $Me_3P[PhPdX]PMe_3$ species. The latter are resistant to capture, thus preventing the formation of the Pd (1 1 1) surface (N_{max} = 11−12, Table 5, rows 6 and 10), which is the most stable surface of metallic Pd.[100]

Palladium halide $[Pd_nX_{2n}]$ species that are significantly more stable than $[PhPdX]_n$ are further stabilized by X^- (X = Br, I) binding (see Table 5 and the Supporting Information). Anionic $[PdBr_3]^-$ is stable against recapture that would lead to the formation of the Pd (1 0 0) surface, while $[PdI_3]^-$ (N_{max} = 10) is stable against being captured as an atom of the Pd (1 1 1) surface (N_{broken} = 9). Such stability of $X[Pd_nX_{2n}]X^{2-}$ species could make them inactive; the activity can be restored by a steady reduction of the halide species in the course of the reaction.

The oligomerization of leached species and additional ligand binding should be considered as simultaneous processes for the sake of model adequacy. We modeled the processes and depicted some representative structures of the resulting $L[PhPdI]_2L$ (L = I^-, NMe_3, and PMe_3), $L[PhPdI]_4L$ (L = I^-), and $I[Pd_nI_{2n}]I^{2-}$ species in Figure 7 (see all considered cases in the Supporting Information). No qualitative change in the $[PhPdX]_n$ moiety upon additional ligand binding was found except in the case of NMe_3 binding to $[PhPdX]_n$ (2Ph-μ). Here, the spontaneous formation of Ph−Ph occurred, and the formed biphenyl molecule became a bridging ligand instead of two μ_2-Ph ligands (Figure 7a). Notably, the resulting molecule comprises Pd atoms in the formal oxidation state +1, and this simple reaction may be a pathway to the formation of Pd(I) species observed in cross-coupling reactions.[132,133]

The combined stabilizing effect of oligomerization and additional ligand binding may be illustrated by the plots depicted in Figure 8. If a Pd catalytic system is "ligandless" and no amine is added as a base, the oligomerization alone is insufficient to prevent the recapture. Among the examined $[PhPdBr]_n$ oligomers, only cyclic tetramer $[PhPdBr]_n$ was stable enough against the capture (Figure 8a), while $[PhPdI]_n$ oligomers were rather stable at $n > 3$ (that is, the N_{max}/n metric was above the 4.5 margin). In the absence of NR_3 or PR_3 ligands, halide anions (formed upon the reaction progress or introduced as an additive) may sufficiently stabilize $X-[PhPdX]_nX^{2-}$ oligomers as indicated by the corresponding N_{max}/n stability metric values of about 5. Indeed, PdNPs having surface Pd atoms bound to 4−5 atoms each (N_{max} = 4−5) were shown to be exceptionally active in the Suzuki cross-

DOI: 10.1021/acscatal.9b00207
ACS Catal. 2019, 9, 3991−4005

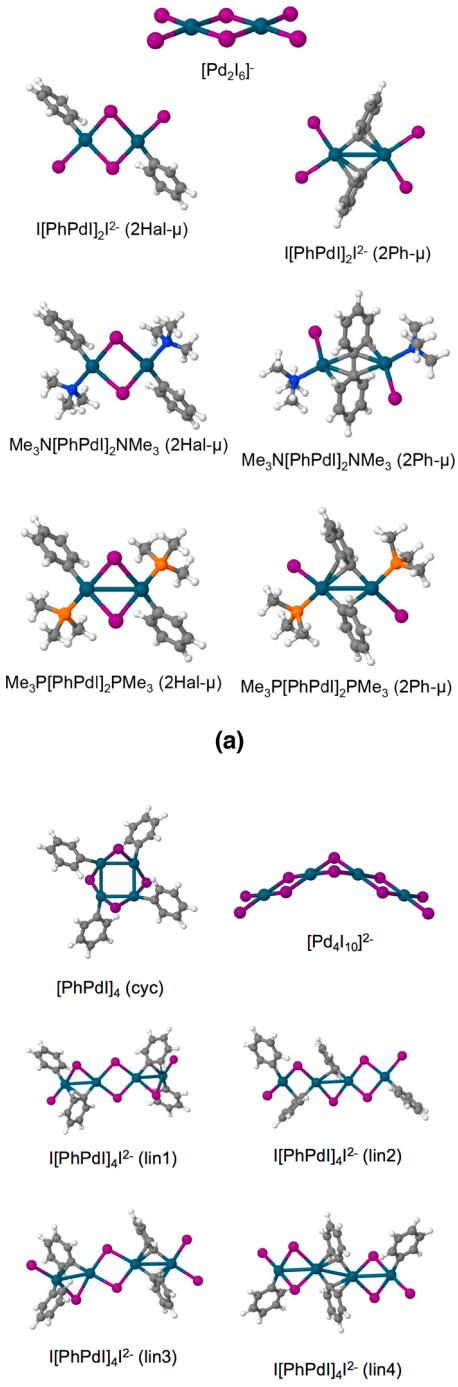

Figure 7. Optimized structures of (a) dimeric Pd intermediates in reactions with PhI and (b) tetrameric Pd intermediates in reactions with PhI. Pd is shown in cerulean, H in white, C in gray, N in blue, P in orange, and I in violet.

coupling reaction with no ligands or amine base added; the exceptional activity was attributed to facile leaching of Pd from these nanoparticles.[37,55]

The modeled $X[PhPdX]_{2-4}X^{2-}$ oligomers and $[PhPdX_2]^-$ monomer had similar stability against the capture (N_{max} = 5–6); therefore, long $X[PhPdX]_nX^{2-}$ chains most likely decompose to mono- and dipalladium species in the presence of excess X^- (since only monomers and dimers X-

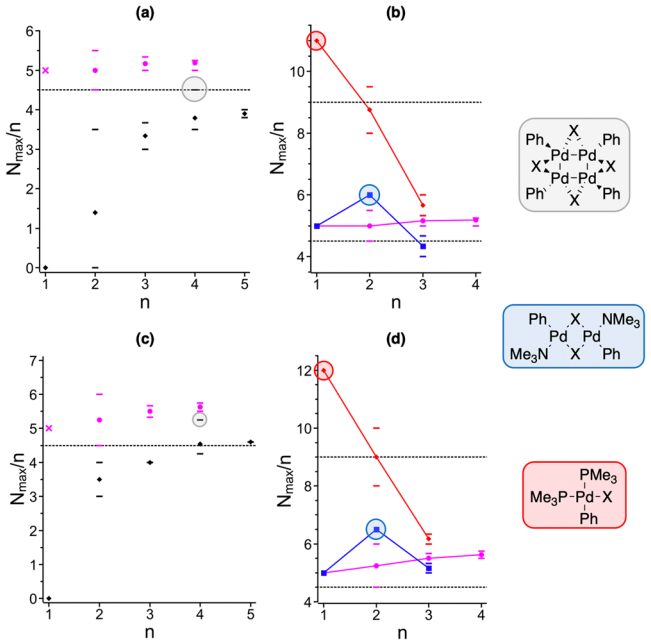

Figure 8. Dependence of species stability (N_{max}/n) on the oligomerization degree (n): (a) stability of $[PhPdBr]_n$ (black diamonds) and $Br[PhPdBr]_nBr^{2-}$ (magenta disks); (b) stability of $Br[PhPdBr]_nBr^{2-}$ (magenta disks), $Me_3N[PhPdBr]_nNMe_3$ (blue squares), and $Me_3P[PhPdBr]_nPMe_3$ (red diamonds); (c) stability of $[PhPdI]_n$ (black diamonds) and $I[PhPdI]_nI^{2-}$ (magenta disks); (d) stability of $I[PhPdI]_nI^{2-}$ (magenta disks), $Me_3N[PhPdI]_nNMe_3$ (blue squares), and $Me_3P[PhPdI]_nPMe_3$ (red diamonds). The stability metric of $[PhPdX_2]^-$ anions is given as magenta crosses on (a) and (c). Error bars indicate the highest and lowest calculated N_{max}/n values for a given n value. The structures of the most stable intermediates are depicted on the right, and the corresponding N_{max}/n values are marked with circles of the corresponding color. Horizontal dotted lines at N_{max}/n values of 4.5 and 9 depict stability margins (stable under reaction conditions and resistant to the capture (leached irreversibly), respectively).

$[PhPdX]_{1-2}X^{2-}$ have a [PhPdX] to X^- ratio of 1:1). The high stability of the anionic species stresses the importance of considering anionic mechanisms in Pd-catalyzed reactions of C–C- and C–heteroatom bond formation as has been proposed (primarily for the Heck reaction,[70,101,134–136] but for other catalytic transformations as well).[137–140]

Capping $[PhPdX]_n$ oligomers with PMe_3 effectively stabilized the species due to the high binding affinity (E_{bind}) of the ligand. However, this effect was reduced by oligomerization, as E_{oligo} was significantly lower than E_{bind} of PMe_3; as a result, the N_{max}/n value dropped with increasing n (Figure 8b,d). The well-known bis-phosphine $Me_3P[PhPdX]$-PMe_3 (X = Br, I) complexes are highly stable and form under reaction conditions. At the same time, dimeric Me_3P-$[PhPdX]_2PMe_3$ (2X-μ) species have also been considered in theoretical studies[141,142] and observed experimentally.[127,128,143] Even $Me_3P[PhPdX]_3PMe_3$ species are somewhat more stable than their anionic $X[PhPdX]_3X^{2-}$ counterparts. Evidently, $R_3P[PhPdX]_{1-3}PR_3$ are important intermediates in Pd catalytic systems containing phosphine ligands. As long as PR_3 ligands are bound to the opposite sides of the $[PhPdX]_{2-3}$ chains, no significant destabilization by ligand steric repulsion (which is known to be a short-range effect) should be expected.

The PMe_3 to Pd ratio in the $Me_3P[PhPdX]_nPMe_3$ oligomers should be discussed. If the ligand is in a 2-fold excess (2:1),

DOI: 10.1021/acscatal.9b00207
ACS Catal. 2019, 9, 3991–4005

$R_3P[PhPdX]_1PR_3$ species, which are highly stable against the capture, drive the conventional Pd(0)/Pd(II) catalytic process. Often the 1:1 ratio is optimal;[144−146] however, the concomitant formation of the $R_3P[PhPdX]_2PR_3$ dimers is an undesirable event.[141] Lowering the ratio to 3:2 may lead to the formation of $R_3P[PhPdX]_3PR_3$ trimers that are considerably less stable against the capture. The lower stability of the trimers may favor the formation of a "cocktail"-type catalytic system where PdNPs, base- and additive-stabilized species as $Me_3N[PhPdX]_nNMe_3$, and $X[PhPdX]_nX^{2-}$ coexist (as they have close stability metric N_{max}/n values for n = 3, Figure 8b,d).

The dimeric 2X-μ-species are the most stable in the $Me_3N[PhPdX]_nNMe_3$ row, while trimeric Me_3N-$[PhPdX]_3NMe_3$ species are less stable than $X[PhPdX]_3X^{2-}$, according to the computations (Figure 8b,d). Since binding of two trimethylamine ligands to $[PhPdX]_2$ (2Ph-μ) complex caused spontaneous formation of Ph−-Ph, we excluded $Me_3N[PhPdX]_2NMe_3$ (2Ph-μ) from the data presented in Figure 8. The role of amine base in Pd-catalyzed cross-coupling and functionalization reactions may thus be dual: as an agent that directs leached [ArPdX] from the deactivation pathway resulting in $[Pd_nX_{2n}]$ formation (red sector in Figure 8) and as a ligand that stabilizes $Me_3N[PhPdX]_{1-2}NMe_3$ when no other ligand is added to a catalytic system to stabilize Pd in solution.

On the basis of the presented modeling, we consider $X[PhPdX]_{1-2}X^{2-}$, $R_3P[PhPdX]_{1-3}PR_3$, and R_3N-$[PhPdX]_{1-2}NR_3$ as important intermediates that represent the pool of the "leached Pd". The relative stability of these intermediates, however, may depend on reaction conditions. For example, in the case of the Heck reaction with aryl bromides, $Br[ArPdBr]_2Br^{2-}$ is known to be stable due to the formation of HBr and the concomitant protonation of NR_3 and PR_3.[102]

Palladium halides $[Pd_nX_{2n}]$ (X = Br, I) are effectively stabilized against the recapture via oligomerization alone (Figure 9); the stability (N_{max}/n) monotonically increases with the rise of the oligomerization degree (n). The dependence of N_{max}/n on n may be extrapolated by the function

$$\frac{N_{max}}{n} = \frac{c}{n} + N_{poly}$$

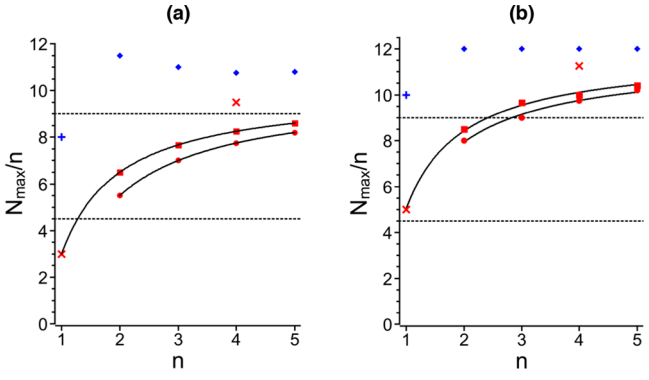

Figure 9. Stability of $[PdX_2]_n$ (trans), $[PdX_2]_n$ (cis), and $[Pd_nX_{2n+2}]^{2-}$ (red squares, red disks, and blue diamonds, respectively): (a) X = Br; (b) X= I. Stability metrics of PdX_2 and $[Pd_4X_8]$ (cyc) are given as red crosses, and the stability metrics of $[PdX_3]^-$ as blue crosses. Horizontal dotted lines at N_{max}/n values of 4.5 and 9 depict stability margins (stable under reaction conditions and stable against the capture (leached irreversibly), respectively).

where c is a fitting coefficient and N_{poly} is N_{max}/n of the polymeric $PdBr_2$ or PdI_2 chains. We excluded $[PdX_3]^-$ from the fit in the case of $[Pd_nX_{2n}]$ cis oligomerization, as the inclusion deteriorated the fit. This may be an indication that the terminal Pd atom in $[Pd_nX_{2n}]$ (cis) chains has an oxidation state other than II due to the unsaturated valence shell. Cyclic $[Pd_4X_8]$ (cyc) tetramers have higher stability than their linear counterparts $[Pd_4X_8]$ (Figure 9, cyclic tetramers are marked with red crosses). However, cyclic tetramers $[Pd_4X_8]$ (cyc) are unstable toward the formation of linear dianionic tetramers $[Pd_nX_{2n+2}]^{2-}$ (Figure 9, see also the structures (150)−(153) and (158)−(161) in the Supporting Information). It should be noted that the presented model of polymeric Pd halides does not account for the formation of the bulk PdX_2 phase and treats the PdX_2 polymeric chain as well dissolved in the DMF solvent. Accounting for the cohesive energy of PdX_2 chains through explicit modeling of the PdX_2 bulk might increase Pd halide stability even more but is beyond the scope of this work.

Capping of the halide chains with X^- anions makes them exceptionally stable. Particularly, bromide oligomers $[Pd_nBr_{2n+2}]^{2-}$ have an N_{max}/n metric value of ca. 11 and their iodide analogues $[Pd_nI_{2n+2}]^{2-}$ have the maximal possible stability (since N_{max}/n = 12 is the maximal number of broken Pd−Pd bonds corresponding to a *hypothetical* process of Pd atom abstraction from Pd bulk, N_{max}/n = 12 was chosen as a cutoff value in the N_{max}/n calculations). The dimeric bromide $[Pd_2I_6]^{2-}$ has the highest stability among the oligomeric dianions and is another form of deactivated Pd in reactions with ArBr (along with Pd bulk and $PdBr_2$) under the excess of the Br^- anions in the system. The stability metric N_{max}/n of $[Pd_nI_{2n+2}]^{2-}$ (n = 2−5) is over the scale (no peak under n = 2 in Figure 9b as in Figure 9a); however, the $[Pd_2I_6]^{2-}$ anion was observed in the Heck reaction,[101] and therefore the same anionic di-Pd species are relevant for the reactions with ArI. Active Pd species thus may undergo conversion to halides such as $[Pd_2X_6]^{2-}$ and the polymeric PdX_2 bulk; we propose that the conversion may proceed via the aforementioned homocoupling of ArX and formation of Pd(IV) complexes (Figure 5). As long as PdX_2 salts are often used as precatalysts that require activation (reduction), the ArX homocoupling not only increases the byproduct formation but also lowers the system activity.

4. CONCLUSIONS

We have evaluated the roles of metal leaching and recapture in a model system that involves ArX oxidative addition as a key mechanistic step. Chemical transformations of different Pd forms analyzed in this work can be encountered in cross-couplings and C−H arylations, as well as in the Heck reaction and Buchwald−Hartwig amination (Figure 10). We understand leaching as a process where the endothermic effect of metallic Pd−Pd bond breaking can be counterbalanced by the cumulative exothermic effect of covalent/coordination bond formation, including coordination to ligands, ArX oxidative addition, and oligomerization of soluble Pd species. The resistance of Pd nanoparticles to dissolution in the course of the reaction may indicate incomplete compensation of the thermodynamic effects. In this case, the overall thermodynamic effect corresponding to the leaching−capture equilibrium may be endergonic (section 3.1).

In practice, sigmoidal reaction kinetics is often observed in cross-coupling and functionalization reactions when a metal-complex palladium precatalyst is used. This is commonly

DOI: 10.1021/acscatal.9b00207
ACS Catal. 2019, 9, 3991−4005

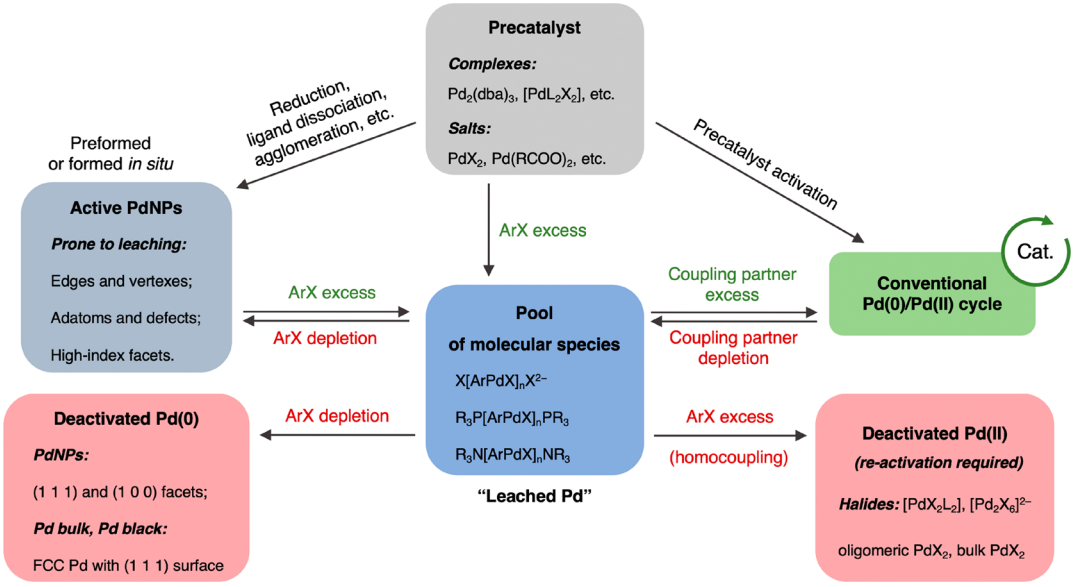

Figure 10. Proposed model of evolution of Pd catalytic systems in reactions that involve ArX oxidative addition.

attributed to the obligate formation of Pd nanoparticles that serve as a pool of catalytically active Pd(0).[47] The observed sigmoidal kinetics, apparently related to the slow ligand loss, may also reflect the reduction of Pd(II) precatalyst and the formation of molecular L[ArPd(II)X]$_n$L species (marked in blue in Figure 10). Therefore, in Pd-catalyzed reactions that involve ArX reagents, three *pools* of species depicted in Figure 10 (Pd(0) nanoparticles, molecular Pd species, and inactive Pd) should be considered irrespective of precatalyst choice. The pool of "leached Pd" corresponds to resting states of the catalyst. According to the results of the modeling, this pool may consist of X[PhPdX]$_{1-2}$X^{2-}, R$_3$P[PhPdX]$_{1-3}$PR$_3$, and R$_3$N[PhPdX]$_{1-2}$NR$_3$ species, depending on reaction type (the Heck reaction, cross-coupling, etc.) and specific reaction conditions (ligand/ligandless system, salt additives).

The present computational study highlighted a number of pathways for dynamic interconversions of palladium complexes, clusters, and nanoparticles. The high level of complexity appears to be a specific feature of cross-coupling catalysis and several other catalytic transformations, where computational modeling provides a unique opportunity to get valuable insight into the reaction mechanism. We, pursuing a unified theory of dynamic "cocktail"-type catalytic systems, studied the energetics of leaching as a first step to theoretically address this complexity.

The high complexity of the studied system imposes some limitations to computational modeling that should be pointed out. For example, calculation of free energies, explicit consideration of solvent molecules, selection of a higher level of theory, and molecular dynamics on full-size models can further improve our understanding. Reliable modeling of catalyst transformation kinetics is also crucial for future progress in this area. Any of the elementary reactions, revealed in the present calculations of "cocktail"-type systems, can be addressed individually in more detail using sophisticated computational methods. We thus anticipate future studies systematically addressing dynamic transformations in Pd catalytic systems.

■ ASSOCIATED CONTENT

Supporting Information

The Supporting Information is available free of charge on the ACS Publications website at DOI: 10.1021/acscatal.9b00207.

Detailed description of the chosen computational parameters and mathematical formulas used, as well as the obtained structures and energy values (PDF)

Optimized structures (ZIP)

■ AUTHOR INFORMATION

Corresponding Author

*E-mail for M.V.P.: M.Polynskii@tudelft.nl, polynskimikhail@gmail.com.

ORCID

Mikhail V. Polynski: 0000-0002-5559-0066

Valentine P. Ananikov: 0000-0002-6447-557X

Notes

The authors declare no competing financial interest.

■ ACKNOWLEDGMENTS

M.V.P. thanks Konstantin Neyman and Sergey Kozlov for useful discussions and NWO Exact and Natural Sciences for the use of supercomputer facilities.

■ REFERENCES

(1) Poree, C.; Schoenebeck, F. A Holy Grail in Chemistry: Computational Catalyst Design: Feasible or Fiction? *Acc. Chem. Res.* **2017**, *50*, 605−608.

(2) Hammes-Schiffer, S. Catalysts by Design: The Power of Theory. *Acc. Chem. Res.* **2017**, *50*, 561−566.

(3) Tantillo, D. J. Faster, Catalyst! React! React! Exploiting Computational Chemistry for Catalyst Development and Design. *Acc. Chem. Res.* **2016**, *49*, 1079.

(4) Jover, J.; Fey, N. The Computational Road to Better Catalysts. *Chem. - Asian J.* **2014**, *9*, 1714−1723.

(5) Eremin, D. B.; Ananikov, V. P. Understanding Active Species in Catalytic Transformations: From Molecular Catalysis to Nanoparticles, Leaching, "Cocktails" of Catalysts and Dynamic Systems. *Coord. Chem. Rev.* **2017**, *346*, 2−19.

DOI: 10.1021/acscatal.9b00207
ACS Catal. 2019, 9, 3991−4005

(6) Balcells, D.; Nova, A. Designing Pd and Ni Catalysts for Cross-Coupling Reactions by Minimizing Off-Cycle Species. *ACS Catal.* **2018**, *8*, 3499−3515.
(7) Suzuki, A.; Yamamoto, Y. Cross-Coupling Reactions of Organoboranes: An Easy Method for C-C Bonding. *Chem. Lett.* **2011**, *40*, 894−901.
(8) Negishi, E.-I.; Zeng, X.; Tan, Z.; Qian, M.; Hu, Q.; Huang, Z. Palladium- or Nickel-Catalyzed Cross-Coupling with Organometals Containing Zinc, Aluminum, and Zirconium: The Negishi Coupling. In *Metal-Catalyzed Cross-Coupling Reactions*; Wiley-VCH: Weinheim, Germany, 2008; pp 815−889.
(9) Oestreich, M. In *The Mizoroki-Heck Reaction*; Oestreich, M., Ed.; Wiley: Chichester, U.K., 2009.
(10) Fortman, G. C.; Nolan, S. P. N-Heterocyclic Carbene (NHC) Ligands and Palladium in Homogeneous Cross-Coupling Catalysis: A Perfect Union. *Chem. Soc. Rev.* **2011**, *40*, 5151.
(11) Haas, D.; Hammann, J. M.; Greiner, R.; Knochel, P. Recent Developments in Negishi Cross-Coupling Reactions. *ACS Catal.* **2016**, *6*, 1540−1552.
(12) Tamao, K.; Sumitani, K.; Kumada, M. Selective Carbon-Carbon Bond Formation by Cross-Coupling of Grignard Reagents with Organic Halides. Catalysis by Nickel-Phosphine Complexes. *J. Am. Chem. Soc.* **1972**, *94*, 4374−4376.
(13) Corriu, R. J. P.; Masse, J. P. Activation of Grignard Reagents by Transition-Metal Complexes. A New and Simple Synthesis of Trans-Stilbenes and Polyphenyls. *J. Chem. Soc., Chem. Commun.* **1972**, *0*, 144a.
(14) Knappke, C. E. I.; Jacobi von Wangelin, A. 35 Years of Palladium-Catalyzed Cross-Coupling with Grignard Reagents: How Far Have We Come? *Chem. Soc. Rev.* **2011**, *40*, 4948.
(15) Sonogashira, K. Development of Pd-Cu Catalyzed Cross-Coupling of Terminal Acetylenes with Sp2-Carbon Halides. *J. Organomet. Chem.* **2002**, *653*, 46−49.
(16) Chinchilla, R.; Nájera, C. Recent Advances in Sonogashira Reactions. *Chem. Soc. Rev.* **2011**, *40*, 5084.
(17) Heck, K. F.; Nolley, J. P. Palladium-Catalyzed Vinylic Hydrogen Substitution Reactions with Aryl, Benzyl, and Styryl Halides. *J. Org. Chem.* **1972**, *37*, 2320−2322.
(18) Mizoroki, T.; Mori, K.; Ozaki, A. Arylation of Olefin with Aryl Iodide Catalyzed by Palladium. *Bull. Chem. Soc. Jpn.* **1971**, *44*, 581−581.
(19) Verrier, C.; Lassalas, P.; Théveau, L.; Quéguiner, G.; Trécourt, F.; Marsais, F.; Hoarau, C. Recent Advances in Direct C-H Arylation: Methodology, Selectivity and Mechanism in Oxazole Series. *Beilstein Journal of Organic Chemistry*; Beilstein-Institut: 2011; pp 1584−1601.
(20) Shibahara, F.; Murai, T. Direct C-H Arylation of Heteroarenes Catalyzed by Palladium/ Nitrogen-Based Ligand Complexes. *Asian J. Org. Chem.* **2013**, *2*, 624−636.
(21) Bohra, H.; Wang, M. Direct C-H Arylation: A "Greener" Approach towards Facile Synthesis of Organic Semiconducting Molecules and Polymers. *J. Mater. Chem. A* **2017**, *5*, 11550−11571.
(22) Reay, A.; Neumann, L.; Fairlamb, I. Catalyst Efficacy of Homogeneous and Heterogeneous Palladium Catalysts in the Direct Arylation of Common Heterocycles. *Synlett* **2016**, *27*, 1211−1216.
(23) Guram, A. S.; Rennels, R. A.; Buchwald, S. L. A Simple Catalytic Method for the Conversion of Aryl Bromides to Arylamines. *Angew. Chem., Int. Ed. Engl.* **1995**, *34*, 1348−1350.
(24) Louie, J.; Hartwig, J. F. Palladium-Catalyzed Synthesis of Arylamines from Aryl Halides. Mechanistic Studies Lead to Coupling in the Absence of Tin Reagents. *Tetrahedron Lett.* **1995**, *36*, 3609−3612.
(25) Ruiz-Castillo, P.; Buchwald, S. L. Applications of Palladium-Catalyzed C-N Cross-Coupling Reactions. *Chem. Rev.* **2016**, *116*, 12564−12649.
(26) Torborg, C.; Beller, M. Recent Applications of Palladium-Catalyzed Coupling Reactions in the Pharmaceutical, Agrochemical, and Fine Chemical Industries. *Adv. Synth. Catal.* **2009**, *351*, 3027−3043.
(27) Magano, J.; Dunetz, J. R. Large-Scale Applications of Transition Metal-Catalyzed Couplings for the Synthesis of Pharmaceuticals. *Chem. Rev.* **2011**, *111*, 2177−2250.
(28) Corbet, J. P.; Mignani, G. Selected Patented Cross-Coupling Reaction Technologies. *Chem. Rev.* **2006**, *106*, 2651−2710.
(29) de Vries, J. G. *Palladium-Catalysed Coupling Reactions*; Springer: Berlin, Heidelberg, 2012; pp 1−34.
(30) Xue, L.; Lin, Z. Theoretical Aspects of Palladium-Catalysed Carbon-Carbon Cross-Coupling Reactions. *Chem. Soc. Rev.* **2010**, *39*, 1692−1705.
(31) Balanta, A.; Godard, C.; Claver, C.; Bunge, M.; Finster, K.; Meyer, R. L.; Skrydstrup, T.; Shafir, A.; Vallribera, A. Pd Nanoparticles for C-C Coupling Reactions. *Chem. Soc. Rev.* **2011**, *40*, 4973.
(32) Lamblin, M.; Nassar-Hardy, L.; Hierso, J. C.; Fouquet, E.; Felpin, F. X. Recyclable Heterogeneous Palladium Catalysts in Pure Water: Sustainable Developments in Suzuki, Heck, Sonogashira and Tsuji-Trost Reactions. *Adv. Synth. Catal.* **2010**, *352*, 33−79.
(33) Ellis, P. J.; Fairlamb, I. J. S.; Hackett, S. F. J.; Wilson, K.; Lee, A. F. Evidence for the Surface-Catalyzed Suzuki-Miyaura Reaction over Palladium Nanoparticles: An Operando XAS Study. *Angew. Chem., Int. Ed.* **2010**, *49*, 1820−1824.
(34) Al-Amin, M.; Honma, T.; Hoshiya, N.; Shuto, S.; Arisawa, M. Ligand-Free Buchwald-Hartwig Aromatic Aminations of Aryl Halides Catalyzed by Low-Leaching and Highly Recyclable Sulfur-Modified Gold-Supported Palladium Material. *Adv. Synth. Catal.* **2012**, *354*, 1061−1068.
(35) Wang, F.; Li, C.; Sun, L.-D.; Wu, H.; Ming, T.; Wang, J.; Yu, J. C.; Yan, C.-H. Heteroepitaxial Growth of High-Index-Faceted Palladium Nanoshells and Their Catalytic Performance. *J. Am. Chem. Soc.* **2011**, *133*, 1106−1111.
(36) Deraedt, C.; Astruc, D. Homeopathic" Palladium Nanoparticle Catalysis of Cross Carbon-Carbon Coupling Reactions. *Acc. Chem. Res.* **2014**, *47*, 494−503.
(37) Collins, G.; Schmidt, M.; O'Dwyer, C.; McGlacken, G.; Holmes, J. D. Enhanced Catalytic Activity of High-Index Faceted Palladium Nanoparticles in Suzuki-Miyaura Coupling Due to Efficient Leaching Mechanism. *ACS Catal.* **2014**, *4*, 3105−3111.
(38) Baumann, C. G.; De Ornellas, S.; Reeds, J. P.; Storr, T. E.; Williams, T. J.; Fairlamb, I. J. S. Formation and Propagation of Well-Defined Pd Nanoparticles (PdNPs) during C-H Bond Functionalization of Heteroarenes: Are Nanoparticles a Moribund Form of Pd or an Active Catalytic Species? *Tetrahedron* **2014**, *70*, 6174−6187.
(39) Pagliaro, M.; Pandarus, V.; Ciriminna, R.; Béland, F.; Demma Carà, P. Heterogeneous versus Homogeneous Palladium Catalysts for Cross-Coupling Reactions. *ChemCatChem* **2012**, *4*, 432−445.
(40) Crabtree, R. H. Resolving Heterogeneity Problems and Impurity Artifacts in Operationally Homogeneous Transition Metal Catalysts. *Chem. Rev.* **2012**, *112*, 1536−1554.
(41) Biffis, A.; Centomo, P.; Del Zotto, A.; Zecca, M. Pd Metal Catalysts for Cross-Couplings and Related Reactions in the 21st Century: A Critical Review. *Chem. Rev.* **2018**, *118*, 2249−2295.
(42) Pla, D.; Gómez, M. Metal and Metal Oxide Nanoparticles: A Lever for C-H Functionalization. *ACS Catal.* **2016**, *6*, 3537−3552.
(43) Ananikov, V. P.; Beletskaya, I. P. Toward the Ideal Catalyst: From Atomic Centers to a "Cocktail" of Catalysts. *Organometallics* **2012**, *31*, 1595−1604.
(44) Kashin, A. S.; Ananikov, V. P. Catalytic C-C and C-Heteroatom Bond Formation Reactions: In Situ Generated or Preformed Catalysts? Complicated Mechanistic Picture behind Well-Known Experimental Procedures. *J. Org. Chem.* **2013**, *78*, 11117−11125.
(45) Hazari, N.; Melvin, P. R.; Beromi, M. M. Well-Defined Nickel and Palladium Precatalysts for Cross-Coupling. *Nat. Rev. Chem.* **2017**, *1*, 0025.
(46) Crabtree, R. H. Deactivation in Homogeneous Transition Metal Catalysis: Causes, Avoidance, and Cure. *Chem. Rev.* **2015**, *115*, 127−150.
(47) Sigeev, A. S.; Peregudov, A. S.; Cheprakov, A. V.; Beletskaya, I. P. The Palladium Slow-Release Pre-Catalysts and Nanoparticles in the

DOI: 10.1021/acscatal.9b00207
ACS Catal. 2019, 9, 3991−4005

"Phosphine-Free" Mizoroki-Heck and Suzuki-Miyaura Reactions. *Adv. Synth. Catal.* **2015**, *357*, 417−429.
(48) Astakhov, A. V.; Khazipov, O. V.; Chernenko, A. Y.; Pasyukov, D. V.; Kashin, A. S.; Gordeev, E. G.; Khrustalev, V. N.; Chernyshev, V. M.; Ananikov, V. P. A New Mode of Operation of Pd-NHC Systems Studied in a Catalytic Mizoroki-Heck Reaction. *Organometallics* **2017**, *36*, 1981−1992.
(49) Canseco-Gonzalez, D.; Gniewek, A.; Szulmanowicz, M.; Müller-Bunz, H.; Trzeciak, A. M.; Albrecht, M. PEPPSI-Type Palladium Complexes Containing Basic 1,2,3-Triazolylidene Ligands and Their Role in Suzuki-Miyaura Catalysis. *Chem. - Eur. J.* **2012**, *18*, 6055−6062.
(50) Górna, M.; Szulmanowicz, M. S.; Gniewek, A.; Tylus, W.; Trzeciak, A. M. Recyclable Pd(0)-Pd(II) Composites Formed from Pd(II) Dimers with NHC Ligands under Suzuki-Miyaura Conditions. *J. Organomet. Chem.* **2015**, *785*, 92−99.
(51) Chernyshev, V. M.; Khazipov, O. V.; Shevchenko, M. A.; Chernenko, A. Y.; Astakhov, A. V.; Eremin, D. B.; Pasyukov, D. V.; Kashin, A. S.; Ananikov, V. P. Revealing the Unusual Role of Bases in Activation/Deactivation of Catalytic Systems: O-NHC Coupling in M/NHC Catalysis. *Chem. Sci.* **2018**, *9*, 5564−5577.
(52) Khazipov, O. V.; Shevchenko, M. A.; Chernenko, A. Y.; Astakhov, A. V.; Pasyukov, D. V.; Eremin, D. B.; Zubavichus, Y. V.; Khrustalev, V. N.; Chernyshev, V. M.; Ananikov, V. P. Fast and Slow Release of Catalytically Active Species in Metal/NHC Systems Induced by Aliphatic Amines. *Organometallics* **2018**, *37*, 1483−1492.
(53) Biffis, A.; Zecca, M.; Basato, M. Metallic Palladium in the Heck Reaction: Active Catalyst or Convenient Precursor? *Eur. J. Inorg. Chem.* **2001**, *2001*, 1131−1133.
(54) de Vries, J. G. When Does Catalysis with Transition Metal Complexes Turn into Catalysis by Nanoparticles? In *Selective Nanocatalysts and Nanoscience*; Wiley-VCH: Weinheim, Germany, 2011; pp 73103.
(55) Collins, G.; Schmidt, M.; O'Dwyer, C.; Holmes, J. D.; McGlacken, G. P. *Angew. Chem., Int. Ed.* **2014**, *53*, 4142−4145.
(56) Leyva-Pérez, A.; Oliver-Meseguer, J.; Rubio-Marqués, P.; Corma, A. *Angew. Chem., Int. Ed.* **2013**, *52*, 11554−11559.
(57) Trzeciak, A. M.; Ziółkowski, J. J. Structural and Mechanistic Studies of Pd-Catalyzed C-C Bond Formation: The Case of Carbonylation and Heck Reaction. *Coord. Chem. Rev.* **2005**, *249*, 2308−2322.
(58) Trzeciak, A. M.; Ziółkowski, J. J. Monomolecular, Nanosized and Heterogenized Palladium Catalysts for the Heck Reaction. *Coord. Chem. Rev.* **2007**, *251*, 1281−1293.
(59) Goldbach, V.; Krumova, M.; Mecking, S. Full-Range Interconversion of Nanocrystals and Bulk Metal with a Highly Selective Molecular Catalyst. *ACS Catal.* **2018**, *8*, 5515−5525.
(60) Sperger, T.; Sanhueza, I. A.; Schoenebeck, F. Computation and Experiment: A Powerful Combination to Understand and Predict Reactivities. *Acc. Chem. Res.* **2016**, *49*, 1311−1319.
(61) Sperger, T.; Fisher, H. C.; Schoenebeck, F. Computationally Deciphering Palladium-Catalyzed Reaction Mechanisms. *Wiley Interdiscip. Rev. Comput. Mol. Sci.* **2016**, *6*, 226−242.
(62) Sperger, T.; Sanhueza, I. A.; Kalvet, I.; Schoenebeck, F. Computational Studies of Synthetically Relevant Homogeneous Organometallic Catalysis Involving Ni, Pd, Ir, and Rh: An Overview of Commonly Employed DFT Methods and Mechanistic Insights. *Chem. Rev.* **2015**, *115*, 9532−9586.
(63) García-Melchor, M.; Braga, A. A. C.; Lledós, A.; Ujaque, G.; Maseras, F. Computational Perspective on Pd-Catalyzed C-C Cross-Coupling Reaction Mechanisms. *Acc. Chem. Res.* **2013**, *46*, 2626−2634.
(64) Veerakumar, P.; Thanasekaran, P.; Lu, K.-L.; Lin, K.-C.; Rajagopal, S. Computational Studies of Versatile Heterogeneous Palladium-Catalyzed Suzuki, Heck, and Sonogashira Coupling Reactions. *ACS Sustainable Chem. Eng.* **2017**, *5*, 8475−8490.
(65) Ramezani-Dakhel, H.; Mirau, P. A.; Naik, R. R.; Knecht, M. R.; Heinz, H. Stability, Surface Features, and Atom Leaching of Palladium Nanoparticles: Toward Prediction of Catalytic Functionality. *Phys. Chem. Chem. Phys.* **2013**, *15*, 5488.
(66) Bedford, N. M.; Ramezani-Dakhel, H.; Slocik, J. M.; Briggs, B. D.; Ren, Y.; Frenkel, A. I.; Petkov, V.; Heinz, H.; Naik, R. R.; Knecht, M. R. Elucidation of Peptide-Directed Palladium Surface Structure for Biologically Tunable Nanocatalysts. *ACS Nano* **2015**, *9*, 5082−5092.
(67) Briggs, B. D.; Bedford, N. M.; Seifert, S.; Koerner, H.; Ramezani-Dakhel, H.; Heinz, H.; Naik, R. R.; Frenkel, A. I.; Knecht, M. R.; Knecht, M. R. Atomic-Scale Identification of Pd Leaching in Nanoparticle Catalyzed C-C Coupling: Effects of Particle Surface Disorder. *Chem. Sci.* **2015**, *6*, 6413−6419.
(68) Heinz, H.; Pramanik, C.; Heinz, O.; Ding, Y.; Mishra, R. K.; Marchon, D.; Flatt, R. J.; Estrela-Lopis, I.; Llop, J.; Moya, S.; Ziolo, R. F. Nanoparticle Decoration with Surfactants: Molecular Interactions, Assembly, and Applications. *Surf. Sci. Rep.* **2017**, *72*, 1−58.
(69) Zvereva, E. E.; Katsyuba, S. A.; Dyson, P. J.; Aleksandrov, A. V. Leaching from Palladium Nanoparticles in an Ionic Liquid Leads to the Formation of Ionic Monometallic Species. *J. Phys. Chem. Lett.* **2017**, *8*, 3452−3456.
(70) de Vries, J. G. A Unifying Mechanism for All High-Temperature Heck Reactions. The Role of Palladium Colloids and Anionic Species. *Dalt. Trans.* **2006**, *0*, 421−429.
(71) Xu, J.; Wilson, A. R.; Rathmell, A. R.; Howe, J.; Chi, M.; Wiley, B. J. Synthesis and Catalytic Properties of Au-Pd Nanoflowers. *ACS Nano* **2011**, *5*, 6119−6127.
(72) Perdew, J. P.; Burke, K.; Ernzerhof, M. Generalized Gradient Approximation Made Simple. *Phys. Rev. Lett.* **1996**, *77*, 3865−3868.
(73) Kresse, G.; Furthmüller, J. *Efficient Iterative Schemes for* Ab Initio *Total-Energy Calculations Using a Plane-Wave Basis Set. Phys. Rev. B: Condens. Matter Mater. Phys.* **1996**, *54*, 11169−11186.
(74) Kresse, G.; Joubert, D. From Ultrasoft Pseudopotentials to the Projector Augmented-Wave Method. *Phys. Rev. B: Condens. Matter Mater. Phys.* **1999**, *59*, 1758−1775.
(75) Monkhorst, H.; Pack, J. Special Points for Brillouin-Zone Integrations. *Phys. Rev. B* **1976**, *13*, 5188−5192.
(76) Mermin, N. D. Thermal Properties of the Inhomogeneous Electron Gas. *Phys. Rev.* **1965**, *137*, A1441−A1443.
(77) Neese, F. The ORCA Program System. *Wiley Interdiscip. Rev. Comput. Mol. Sci.* **2012**, *2*, 73−78.
(78) Baerends, E. J.; Ellis, D. E.; Ros, P. Self-Consistent Molecular Hartree—Fock—Slater Calculations I. The Computational Procedure. *Chem. Phys.* **1973**, *2*, 41−51.
(79) Dunlap, B. I.; Connolly, J. W. D.; Sabin, J. R. On Some Approximations in Applications of $X\alpha$ Theory. *J. Chem. Phys.* **1979**, *71*, 3396.
(80) Van Alsenoy, C. Ab Initio Calculations on Large Molecules: The Multiplicative Integral Approximation. *J. Comput. Chem.* **1988**, *9*, 620−626.
(81) Kendall, R. A.; Früchtl, H. A. The Impact of the Resolution of the Identity Approximate Integral Method on Modern Ab Initio Algorithm Development. *Theor. Chem. Acc.* **1997**, *97*, 158−163.
(82) Eichkorn, K.; Weigend, F.; Treutler, O.; Ahlrichs, R. Auxiliary Basis Sets for Main Row Atoms and Transition Metals and Their Use to Approximate Coulomb Potentials. *Theor. Chem. Acc.* **1997**, *97*, 119−124.
(83) Eichkorn, K.; Treutler, O.; Öhm, H.; Häser, M.; Ahlrichs, R. Auxiliary Basis Sets to Approximate Coulomb Potentials. *Chem. Phys. Lett.* **1995**, *240*, 283−289.
(84) Whitten, J. L. Coulombic Potential Energy Integrals and Approximations. *J. Chem. Phys.* **1973**, *58*, 4496.
(85) Andrae, D.; Häußermann, U.; Dolg, M.; Stoll, H.; Preuß, H. Energy-Adjusted Ab Initio Pseudopotentials for the Second and Third Row Transition Elements. *Theor. Chim. Acta* **1990**, *77*, 123−141.
(86) Peterson, K. A.; Figgen, D.; Goll, E.; Stoll, H.; Dolg, M. *Systematically Convergent Basis Sets with Relativistic Pseudopotentials. II. Small-Core Pseudopotentials and Correlation Consistent Basis Sets for the Post-* d *Group 16−18 Elements. J. Chem. Phys.* **2003**, *119*, 11113−11123.

DOI: 10.1021/acscatal.9b00207
ACS Catal. 2019, 9, 3991−4005

(87) Klamt, A.; Schüürmann, G. COSMO: A New Approach to Dielectric Screening in Solvents with Explicit Expressions for the Screening Energy and Its Gradient. *J. Chem. Soc., Perkin Trans. 2* **1993**, *0*, 799−805.
(88) Janthon, P.; Luo, S.; Kozlov, S. M.; Vines, F.; Limtrakul, J.; Truhlar, D. G.; Illas, F. Bulk Properties of Transition Metals: A Challenge for the Design of Universal Density Functionals. *J. Chem. Theory Comput.* **2014**, *10*, 3832−3839.
(89) Vines, F.; Gomes, J. R. B.; Illas, F. Understanding the Reactivity of Metallic Nanoparticles: Beyond the Extended Surface Model for Catalysis. *Chem. Soc. Rev.* **2014**, *43*, 4922−4939.
(90) Chen, M.; Craciun, R.; Hoffman, N.; Dixon, D. a. *Inorg. Chem.* **2012**, *51*, 13195−13203.
(91) Jacobsen, H.; Cavallo, L. On the Accuracy of DFT Methods in Reproducing Ligand Substitution Energies for Transition Metal Complexes in Solution: The Role of Dispersive Interactions. *ChemPhysChem* **2012**, *13*, 562−569.
(92) Kovács, G.; Stirling, A.; Lledós, A.; Ujaque, G. The Nature of $[PdCl_2(C_2H_4)(H_2O)]$ as an Active Species in the Wacker Process: New Insights from Ab Initio Molecular Dynamics Simulations. *Chem. - Eur. J.* **2012**, *18*, 5612−5619.
(93) Stirling, A.; Nair, N. N.; Lledós, A.; Ujaque, G. Challenges in Modelling Homogeneous Catalysis: New Answers from Ab Initio Molecular Dynamics to the Controversy over the Wacker Process. *Chem. Soc. Rev.* **2014**, *43*, 4940−4952.
(94) Vidossich, P.; Ujaque, G.; Lledós, A. Palladium Monophosphine $Pd(PPh_3)$: Is It Really Accessible in Solution? *Chem. Commun.* **2014**, *50*, 661−663.
(95) Vidossich, P.; Lledós, A.; Ujaque, G. *Realistic Simulation of Organometallic Reactivity in Solution by Means of First-Principles Molecular Dynamics*; Springer International: Cham, Switzerland, 2015; pp 81−106.
(96) Vidossich, P.; Lledós, A.; Ujaque, G. First-Principles Molecular Dynamics Studies of Organometallic Complexes and Homogeneous Catalytic Processes. *Acc. Chem. Res.* **2016**, *49*, 1271−1278.
(97) Zvereva, E. E.; Katsyuba, S. A.; Dyson, P. J.; Aleksandrov, A. V. Solvation of Palladium Clusters in an Ionic Liquid: A QM/MM Molecular Dynamics Study. *J. Phys. Chem. C* **2016**, *120*, 4596−4604.
(98) Besora, M.; Vidossich, P.; Lledós, A.; Ujaque, G.; Maseras, F. Calculation of Reaction Free Energies in Solution: A Comparison of Current Approaches. *J. Phys. Chem. A* **2018**, *122*, 1392−1399.
(99) Plata, R. E.; Singleton, D. A. A Case Study of the Mechanism of Alcohol-Mediated Morita Baylis-Hillman Reactions. The Importance of Experimental Observations. *J. Am. Chem. Soc.* **2015**, *137*, 3811−3826.
(100) Popa, C.; Zhu, T.; Tranca, I.; Kaghazchi, P.; Jacob, T.; Hensen, E. J. M.; Kaghazchi, P.; Balmes, O.; van Rijn, R.; Deppert, K.; Bluhm, H.; Liu, Z.; Grass, M. E.; Hävecker, M.; Lundgren, E. Structure of Palladium Nanoparticles under Oxidative Conditions. *Phys. Chem. Chem. Phys.* **2015**, *17*, 2268−2273.
(101) Evans, J.; O'Neill, L.; Kambhampati, V. L.; Rayner, G.; Turin, S.; Genge, A.; Dent, A. J.; Neisius, T.; Macleod, D. N.; Ramsdale, C. M.; Salvini, G. Structural Characterisation of Solution Species Implicated in the Palladium-Catalysed Heck Reaction by Pd K-Edge X-Ray Absorption Spectroscopy: Palladium Acetate as a Catalyst Precursor. *J. Chem. Soc. Dalt. Trans.* **2002**, *1*, 2207−2212.
(102) Carrow, B. P.; Hartwig, J. F. Ligandless, Anionic, Arylpalladium Halide Intermediates in the Heck Reaction. *J. Am. Chem. Soc.* **2010**, *132*, 79−81.
(103) Paul, F.; Patt, J.; Hartwig, J. F. Palladium-Catalyzed Formation of Carbon-Nitrogen Bonds. Reaction Intermediates and Catalyst Improvements in the Hetero Cross-Coupling of Aryl Halides and Tin Amides. *J. Am. Chem. Soc.* **1994**, *116*, 5969−5970.
(104) Widenhoefer, R. A.; Buchwald, S. L. Halide and Amine Influence in the Equilibrium Formation of Palladium Tris(o-Tolyl)Phosphine Mono(Amine) Complexes from Palladium Aryl Halide Dimers. *Organometallics* **1996**, *15*, 2755−2763.
(105) Albéniz, A. C.; Espinet, P.; Martín-Ruiz, B.; Milstein, D. Catalytic System for Heck Reactions Involving Insertion into Pd-(Perfluoro-Organyl) Bonds. *J. Am. Chem. Soc.* **2001**, *123*, 11504−11505.
(106) Rothenberg, G.; Cruz, S. C.; Van Strijdonck, G. P. F.; Hoefsloot, H. C. J. Detailed Mechanistic Studies Using in Situ Spectroscopic Analysis: A Look at Little-Known Regions of the Heck Reaction. *Adv. Synth. Catal.* **2004**, *346*, 467−473.
(107) Albéniz, A. C.; Espinet, P.; Martín-Ruiz, B.; Milstein, D. Catalytic System for the Heck Reaction of Fluorinated Haloaryls. *Organometallics* **2005**, *24*, 3679−3684.
(108) Molina De La Torre, J. A.; Espinet, P.; Albéniz, A. C. Solvent-Induced Reduction of Palladium-Aryls, a Potential Interference in Pd Catalysis. *Organometallics* **2013**, *32*, 5428−5434.
(109) Böck, K.; Feil, J. E.; Karaghiosoff, K.; Koszinowski, K. Catalyst Activation, Deactivation, and Degradation in Palladium-Mediated Negishi Cross-Coupling Reactions. *Chem. - Eur. J.* **2015**, *21*, 5548−5560.
(110) Zhao, F.; Bhanage, B. M.; Shirai, M.; Arai, M. Heck Reactions of Iodobenzene and Methyl Acrylate with Conventional Supported Palladium Catalysts in the Presence of Organic and/or Inorganic Bases without Ligands. *Chem. - Eur. J.* **2000**, *6*, 843−848.
(111) Köhler, K.; Heidenreich, R. G.; Soomro, S. S.; Pröckl, S. S. Supported Palladium Catalysts for Suzuki Reactions: Structure-Property Relationships, Optimized Reaction Protocol and Control of Palladium Leaching. *Adv. Synth. Catal.* **2008**, *350*, 2930−2936.
(112) Köhler, K.; Heidenreich, R. G.; Krauter, J. G. E.; Pietsch, J. Highly Active Palladium/Activated Carbon Catalysts for Heck Reactions: Correlation of Activity, Catalyst Properties, and Pd Leaching. *Chem. - Eur. J.* **2002**, *8*, 622−631.
(113) Conlon, D. A.; Pipik, B.; Ferdinand, S.; LeBlond, C. R.; Sowa, J. R.; Izzo, B.; Collins, P.; Ho, G.-J.; Williams, J. M.; Shi, Y.-J.; Sun, Y. Suzuki-Miyaura Cross-Coupling With Quasi-Heterogeneous Palladium. *Adv. Synth. Catal.* **2003**, *345*, 931−935.
(114) Sun, W.; Liu, Z.; Jiang, C.; Xue, Y.; Chu, W.; Zhao, X. Experimental and Theoretical Investigation on the Interaction between Palladium Nanoparticles and Functionalized Carbon Nanotubes for Heck Synthesis. *Catal. Today* **2013**, *212*, 206−214.
(115) Collins, G.; Holmes, J. D. Engineering Metallic Nanoparticles for Enhancing and Probing Catalytic Reactions. *Adv. Mater.* **2016**, *28*, 5689−5695.
(116) Goossen, L. J.; Koley, D.; Hermann, H. L.; Thiel, W. Palladium Monophosphine Intermediates in Catalytic Cross-Coupling Reactions: A DFT Study. *Organometallics* **2006**, *25*, 54−67.
(117) Li, Z.; Fu, Y.; Guo, Q.-X.; Liu, L. Theoretical Study on Monoligated Pd-Catalyzed Cross-Coupling Reactions of Aryl Chlorides and Bromides. *Organometallics* **2008**, *27*, 4043−4049.
(118) Schoenebeck, F.; Houk, K. N. Ligand-Controlled Regioselectivity in Palladium-Catalyzed Cross Coupling Reactions. *J. Am. Chem. Soc.* **2010**, *132*, 2496−2497.
(119) González-Pérez, A. B.; Álvarez, R.; Faza, O. N.; de Lera, Á. R.; Aurrecoechea, J. M. DFT-Based Insights into Pd-Zn Cooperative Effects in Oxidative Addition and Reductive Elimination Processes Relevant to Negishi Cross-Couplings. *Organometallics* **2012**, *31*, 2053−2058.
(120) Hansmann, M. M.; Pernpointner, M.; Döpp, R.; Hashmi, A. S. K. A Theoretical DFT-Based and Experimental Study of the Transmetalation Step in Au/Pd-Mediated Cross-Coupling Reactions. *Chem. - Eur. J.* **2013**, *19*, 15290−15303.
(121) DelPozo, J.; Gioria, E.; Casares, J. A.; Álvarez, R.; Espinet, P. Organometallic Nucleophiles and Pd: What Makes $ZnMe_2$ Different? Is Au Like Zn? *Organometallics* **2015**, *34*, 3120−3128.
(122) del Pozo, J.; Salas, G.; Álvarez, R.; Casares, J. A.; Espinet, P. The Negishi Catalysis: Full Study of the Complications in the Transmetalation Step and Consequences for the Coupling Products. *Organometallics* **2016**, *35*, 3604−3611.
(123) del Pozo, J.; Pérez-Iglesias, M.; Álvarez, R.; Lledós, A.; Casares, J. A.; Espinet, P. Speciation of $ZnMe_2$, ZnMeCl, and $ZnCl_2$ in Tetrahydrofuran (THF), and Its Influence on Mechanism Calculations of Catalytic Processes. *ACS Catal.* **2017**, *7*, 3575−3583.

DOI: 10.1021/acscatal.9b00207
ACS Catal. 2019, 9, 3991−4005

(124) Wolters, L. P.; Koekkoek, R.; Bickelhaupt, F. M. Role of Steric Attraction and Bite-Angle Flexibility in Metal-Mediated C-H Bond Activation. *ACS Catal.* **2015**, *5*, 5766−5775.
(125) Fu, F.; Xiang, J.; Cheng, H.; Cheng, L.; Chong, H.; Wang, S.; Li, P.; Wei, S.; Zhu, M.; Li, Y. A Robust and Efficient Pd_3 Cluster Catalyst for the Suzuki Reaction and Its Odd Mechanism. *ACS Catal.* **2017**, *7*, 1860−1867.
(126) Astruc, D. Palladium Nanoparticles as Efficient Green Homogeneous and Heterogeneous Carbon-Carbon Coupling Precatalysts: A Unifying View. *Inorg. Chem.* **2007**, *46*, 1884−1894.
(127) Goutierre, A. S.; Trinh, H. V.; Larini, P.; Jazzar, R.; Baudoin, O. Comparative Structural Analysis of Biarylphosphine Ligands in Arylpalladium Bromide and Malonate Complexes. *Organometallics* **2017**, *36*, 129−135.
(128) Ribagnac, P.; Blug, M.; Villa-Uribe, J.; Le Goff, X.-F.; Gosmini, C.; Mézailles, N. Room-Temperature Palladium-Catalyzed Negishi-Type Coupling: A Combined Experimental and Theoretical Study. *Chem. - Eur. J.* **2011**, *17*, 14389−14393.
(129) Matsubara, K.; Yamamoto, H.; Miyazaki, S.; Inatomi, T.; Nonaka, K.; Koga, Y.; Yamada, Y.; Veiros, L. F.; Kirchner, K. Dinuclear Systems in the Efficient Nickel-Catalyzed Kumada-Tamao-Corriu Cross-Coupling of Aryl Halides. *Organometallics* **2017**, *36*, 255−265.
(130) Christmann, U.; Vilar, R.; White, A. J. P.; Williams, D. J. Synthesis of Two Novel Dinuclear Palladium(I) Complexes and Studies of Their Catalytic Activity in Amination Reactions. *Chem. Commun.* **2004**, *0*, 1294−1295.
(131) Barder, T. E. Synthesis, Structural, and Electron Topographical Analyses of a Dialkylbiaryl Phosphine/Arene-Ligated Palladium(I) Dimer: Enhanced Reactivity in Suzuki-Miyaura Coupling Reactions. *J. Am. Chem. Soc.* **2006**, *128*, 898−904.
(132) Aufiero, M.; Scattolin, T.; Proutière, F.; Schoenebeck, F. Air-Stable Dinuclear Iodine-Bridged Pd(I) Complex - Catalyst, Precursor, or Parasite? The Additive Decides. Systematic Nucleophile-Activity Study and Application as Precatalyst in Cross-Coupling. *Organometallics* **2015**, *34*, 5191−5195.
(133) Johansson Seechurn, C. C. C.; Sperger, T.; Scrase, T. G.; Schoenebeck, F.; Colacot, T. J. Understanding the Unusual Reduction Mechanism of Pd(II) to Pd(I): Uncovering Hidden Species and Implications in Catalytic Cross-Coupling Reactions. *J. Am. Chem. Soc.* **2017**, *139*, 5194−5200.
(134) Schmidt, A. F.; Al-Halaiqa, A.; Smirnov, V. V.; Kurokhtina, A. A. State of Palladium in Ligandless Catalytic Systems for the Heck Reaction of Nonactivated Bromobenzene. *Kinet. Catal.* **2008**, *49*, 638−643.
(135) Schroeter, F.; Soellner, J.; Strassner, T. Cross-Coupling Catalysis by an Anionic Palladium Complex. *ACS Catal.* **2017**, *7*, 3004−3009.
(136) Schroeter, F.; Strassner, T. Understanding Anionic "Ligandless" Palladium Species in the Mizoroki-Heck Reaction. *Inorg. Chem.* **2018**, *57*, 5159−5173.
(137) Kozuch, S.; Shaik, S.; Jutand, A.; Amatore, C. Active Anionic Zero-Valent Palladium Catalysts: Characterization by Density Functional Calculations. *Chem. - Eur. J.* **2004**, *10*, 3072−3080.
(138) Kozuch, S.; Amatore, C.; Jutand, A.; Shaik, S. What Makes for a Good Catalytic Cycle? A Theoretical Study of the Role of an Anionic Palladium(0) Complex in the Cross-Coupling of an Aryl Halide with an Anionic Nucleophile. *Organometallics* **2005**, *24*, 2319−2330.
(139) Kozuch, S.; Shaik, S. A Combined Kinetic-Quantum Mechanical Model for Assessment of Catalytic Cycles: Application to Cross-Coupling and Heck Reactions. *J. Am. Chem. Soc.* **2006**, *128*, 3355−3365.
(140) Proutiere, F.; Schoenebeck, F. Solvent Effect on Palladium-Catalyzed Cross-Coupling Reactions and Implications on the Active Catalytic Species. *Angew. Chem., Int. Ed.* **2011**, *50*, 8192−8195.
(141) McMullin, C. L.; Fey, N.; Harvey, J. N. Computed Ligand Effects on the Oxidative Addition of Phenyl Halides to Phosphine Supported Palladium(0) Catalysts. *Dalt. Trans.* **2014**, *43*, 13545−13556.
(142) Moncho, S.; Ujaque, G.; Lledós, A.; Espinet, P. When Are Tricoordinated PdII Species Accessible? Stability Trends and Mechanistic Consequences. *Chem. - Eur. J.* **2008**, *14*, 8986−8994.
(143) Sergeev, A. G.; Zapf, A.; Spannenberg, A.; Beller, M. Synthesis and Crystal Structure of Palladium(0) and Arylpalladium(II) Bromide Complexes of CataCXium A. *Organometallics* **2008**, *27*, 297−300.
(144) Vikse, K.; Naka, T.; McIndoe, J. S.; Besora, M.; Maseras, F. Oxidative Additions of Aryl Halides to Palladium Proceed through the Monoligated Complex. *ChemCatChem* **2013**, *5*, 3604−3609.
(145) Kozuch, S.; Martin, J. M. L. What Makes for a Good Catalytic Cycle? A Theoretical Study of the SPhos Ligand in the Suzuki-Miyaura Reaction. *Chem. Commun.* **2011**, *47*, 4935.
(146) Kozuch, S.; Martin, J. M. L. What Makes for a Bad Catalytic Cycle? A Theoretical Study on the Suzuki-Miyaura Reaction within the Energetic Span Model. *ACS Catal.* **2011**, *1*, 246−253.

DOI: 10.1021/acscatal.9b00207
ACS Catal. 2019, 9, 3991−4005